UC Santa Cruz

UC Santa Cruz Electronic Theses and Dissertations

Title

Functional and Structural Plasticity in the Adult Mammalian Retina After Local Photoreceptor Loss

Permalink

https://escholarship.org/uc/item/87z6t550

Author

Beier, Corinne Natalie

Publication Date

2017

Copyright Information

This work is made available under the terms of a Creative Commons Attribution License, availalbe at https://creativecommons.org/licenses/by/4.0/

Peer reviewed|Thesis/dissertation

eScholarship.org Powered by the California Digital Library
University of California

UNIVERSITY OF CALIFORNIA
SANTA CRUZ

FUNCTIONAL AND STRUCTURAL PLASTICITY IN THE ADULT MAMMALIAN RETINA AFTER LOCAL PHOTORECEPTOR LOSS

A dissertation submitted in partial satisfaction
of the requirements for the degree of

DOCTOR OF PHILOSOPHY

in

ELECTRICAL ENGINEERING

by

Corinne Beier

June 2017

The Dissertation of Corinne Beier is approved:

_____
Professor Alexander Sher, chair

_____
Professor David Feldheim

_____
Professor Joel Kubby

_____
Tyrus Miller
Vice Provost and Dean of Graduate Studies

Copyright © by

Corinne Beier

2017

Table of Contents

List of Figures

ABSTRACT

Functional and Structural Plasticity in the Adult Mammalian Retina After Local Photoreceptor Loss

Corinne Beier

The retina is a thin layer of neural tissue that lines the back of the eye and transforms the visual scene into an electrical signal that is sent to the brain via the optic nerve. The synapse between photoreceptors, the light sensitive neurons, and bipolar cells is the first connection in the retinal circuitry. Loss of photoreceptors during retinal degeneration results in permanent visual loss. Photoreceptor reintroduction has been suggested as a potential approach to sight restoration, but the ability of bipolar cells to establish new functional synapses with photoreceptors is poorly understood. In my work, I investigate if deafferented bipolar cells, i.e. the ones that lost photoreceptors, in the adult mammalian retina can rewire with new photoreceptors. I use focal laser photocoagulation to selectively ablate a small patch of photoreceptors while leaving the rest of the retinal neurons intact. I use electrophysiology recordings of retinal response to visual stimuli to show that the neighboring healthy photoreceptors shift into the ablation zone, thus returning visual sensitivity to the previously deafferented bipolar cells. Furthermore, I use immunohistochemistry to determine if the new synapses of the deafferented bipolar cells are selective for appropriate pre-synaptic partners and investigate the structural mechanisms bipolar cells use to find new partners. I find that deafferented bipolar cells are capable of rewiring correctly with new photoreceptors, but different bipolar

cell types use different rewiring strategies. I also find that the new synapses may not be as selective as those in the healthy retina. These findings support the idea that bipolar cells might be able to synapse with reintroduced photoreceptors, thereby restoring vision in patients blinded by retinal degeneration. However, the diversity of responses to deafferentation between bipolar cell types shows that different parallel pathways have access to different plasticity mechanisms, suggesting that they will respond to photoreceptor reintroduction therapies differently. Improving our understanding of the plasticity within the adult retina is important for the success of future vision restoration therapies.

Dedication

To my parents, Leah and David Beier.

To my sister, Tamara Beier.

To my fiancé, Dennis Gardner.

Acknowledgements

I would like to express my gratitude to my advisor, Professor Alexander Sher, who has supported and mentored me throughout this process. I feel prepared to succeed as a post-doctoral researcher and I attribute that preparation to Sasha. Professor David Feldheim was also influential and supportive. He was always willing to provide constructive criticism and I have learned to appreciate it. Professor Daniel Palanker, was both supportive and encouraging even beyond the scope of our collaborative projects. I'd like to thank Professor Joel Kubby for supporting my research even when it fell outside the realm of electrical engineering.

I would also like to acknowledge previous and current members of the Sher lab who I worked with over the years. Thank you Dr. Erin Zampaglione, Dr. Richard Smith, Dr. Anahit Hovhannisyan and Dr. Arash Ng. I'd also like to thank Sydney Weiser and wish her success on her own path towards a doctorate. Dr. Shinya Ito was always a helpful resource, thank you.

Members of the Feldheim lab were also supportive and provided guidance. Thank you Jena Yamada and Andreea Nistorica for your support and friendship.

I'd like to thank both Dr. Philip Huie and Roopa Dalal for their encouragement and for contributing more than just their hard work to this thesis.

And finally, I'd like to thank Brett Nelson for his enthusiasm and his contributions.

The text of this dissertation includes reprints of the following previously published material: Beier C, Hovhannisyan A, Weiser S, Kung J, Lee S, Yeong Lee

D, Huie P, Dalal R, Palanker D, Sher A (2017) Deafferented adult rod bipolar cells create new synapses with photoreceptors to restore vision. *Journal of Neuroscience*. This dissertation also includes research from the following previously published material: Sher A, Jones BW, Huie P, Paulus YM, Lavinsky D, Leung L-SS, Nomoto H, Beier C, Marc RE, Palanker D (2013) Restoration of Retinal Structure and Function after Selective Photocoagulation. *Journal of Neuroscience*. The co-authors listed in these publications contributed to the research, which forms the basis for part of the dissertation.

INTRODUCTION

The retina is responsible for transforming an animal's visual habitat into neurological signals that can be interpreted by the various visual centers within the brain. As part of this transformation, the visual scene is filtered into parallel neural pathways within the retina. Each pathway must filter the entire visual scene to avoid blind spots, sending the filtered information in parallel to the brain. These pathways are responsible for decoding specific aspects of the visual scene such as color, contrast, and even motion. At least two-dozen parallel pathways are thought to exist within the retina, and recent studies using functional and genetic analyses have added another dozen to this estimate (Sanes and Masland, 2014; Baden et al., 2016). For each parallel pathway to sample the entire visual scene the circuitry within the retina is intertwined and shared between the pathways. During development, circuits are formed and refined in a stereotypic manor such that this interweaving is organized. The specific mechanisms that exist within the developing retina for most of this circuit formation remain a mystery.

Until this thesis, it was unknown whether or not mechanisms existed for stereotyped circuit formation in the adult mammalian retina. Retinal circuitry is stable in adulthood unless confronted with injury or disease, such as photoreceptor degeneration, which causes blindness. Ambitious therapeutic strategies propose to combat blinding diseases by replacing lost cell types, however, it is unknown if the remaining circuitry within the adult retina has the ability to recreate correct circuitry

with new cells. This thesis will begin to explore the mechanisms available to the adult retina for circuit formation and will discuss both the potential and limitations of its innate plastic response.

Neurons and neural terminology

Neurons make up the central nervous system, which includes the retina. Neurons are responsible for grouping collected information to be passed along to other neurons. This flow of information travels from the dendrites, where it is first collected, down the axon to be transferred at the axon terminals. Information is passed from neuron to neuron at synapses in the form of neurotransmitters. A depolarizing change in membrane potential at an axon terminal will release neurotransmitters from the pre-synaptic neuron to be captured by receptors on the dendrites of a post-synaptic neuron. Changes in membrane potential come in two forms: depolarizing or hyperpolarizing. Depolarization or hyperpolarization cause or prevent the release of neurotransmitters, respectively. In most neurons, depolarization initiates an action potential or spike. An action potential is a large and rapid change in membrane potential that travels from the cell body along an axon. Retinal ganglion cells, which are responsible for sending information from the eye to the brain, produce action potentials, which can travel long distances. Retinal ganglion cells, however, are one of the few neurons in the retina that produce action potentials. Bipolar cells and photoreceptors, for example, instead control the release of neurotransmitters through graded potentials (depolarization or hyperpolarization).

Photoreceptors are also unique in that they are sensory neurons; photoreceptors are not post-synaptic to any neurons and instead detect and change their membrane potential in response to light. Photoreceptors are the afferents (pre-synaptic neurons) of bipolar cells. In this thesis I will explore the consequences of bipolar cells becoming deafferented (losing their afferents).

Retina

Light that passes through the cornea and lens is projected onto the back of the eye such that the photoreceptors within the retina can detect photons and convert this detection into an electric potential. The similarities between a camera CCD and a retina end with the photoreceptors. In fact, the comparison between photoreceptors and a CDD is also oversimplified. Photoreceptors are the 'pixels' of the retina, however, there are two types of photoreceptors: rods and cones (Figure 1). Rods are specialized to detect small amounts of light, including single photons, but will saturate at higher light levels. Cones are responsible for light detection in bright environments and are also sensitive to wavelength. Mammals typically have two cones: a short-wavelength sensitive cone (S-cone) and a medium/long-wavelength sensitive cone (M/L-cone). Humans, and some primates, are an exception and have three cones sensitive to short-, medium-, and long-wavelength light (S-, M- and L-cones) (Rowe, 2002). Wavelength sensitivity is dependent on the opsin proteins within a cone photoreceptor (S-, M- or L-opsins). Opsins reside in the outer segments of the cone and upon absorbing a photon change their structure, initiating a signal

cascade within the cell that hyperpolarizes the photoreceptor leading to a reduction in the amount of glutamate released (Burns and Baylor, 2001). Rhodopsin is the rod-equivalent opsin. Cones spread across the entire retina in a mosaic fashion and rod outer segments, which are thinner than their cone counter-parts, are packed between the cones. In this way, both rods and cones capture light from the entire visual scene.

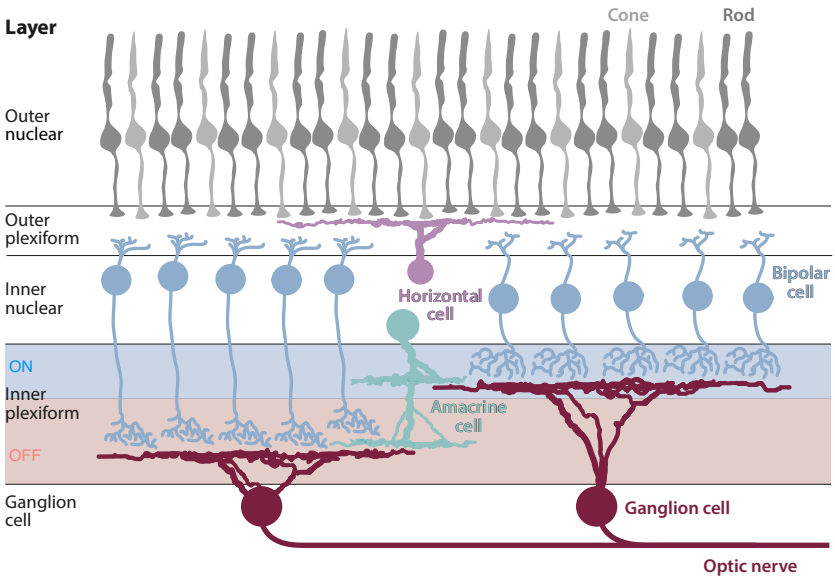

Figure 1. A schematic of retinal neurons.
After passing through the lens of the eye, light is projected through the layers of the retina onto the photoreceptor outer segments, which absorb photons. The outer segments of rods and cones are imbedded in the pigment epithelium (not depicted). Photoreceptors sit in the outer nuclear layer (ONL) of the retina. The spherules and pedicles of rods and cones, respectively, synapse with horizontal and bipolar cells at the outer plexiform layer (OPL). The cell bodies of horizontal, bipolar and amacrine reside in the inner nuclear layer (INL). The inner plexiform layer (IPL) is the synaptic layer between bipolar, amacrine and ganglion cells. ON and OFF bipolar cell axon terminals will stratify in the ON and OFF inner plexiform layers, respectively. The ganglion cell layer (GCL), in addition to ganglion cells, also hosts displaced amacrine cell bodies (not depicted). Ganglion cell axons fasciculate and form the optic tract connecting the retina to the brain. Adapted from (Dhande et al., 2015).

At the outer plexiform layer (OPL) photoreceptors are pre-synaptic to two broad cell classes, bipolar and horizontal cells that are responsible for beginning the parallel pathways within the retina (Figure 1) (reviewed in (Wässle, 2004)). The dendritic trees of horizontal cells, as their name implies, are horizontally oriented within the retina. These cells provide inhibitory feedback onto photoreceptors to modulate their electric potential based on laterally collected information. Horizontal cells are commonly split into two cell types, though this varies by species (Masland, 2012). The two cell types are typically distinguished by their dendritic field size and their selective or non-selective connectivity (Kolb et al., 2016). Bipolar cells are more diverse, exhibiting about a dozen cell types. Bipolar cell types have distinct morphologies, connectivity and, therefore, function within the retina (Euler et al., 2014). For example, the rod bipolar cell is post-synaptic to only rod photoreceptors and therefore is responsible for conveying information at scotopic (dim) light levels. The remaining bipolar cell types are cone bipolar cell types, making connections with cones and sometimes rods. Some cone bipolar cells, named S-cone or M-cone bipolar cells, are exclusively post-synaptic to S- or M-cones, making them functionally selective to S- or M-wavelength stimulus, respectively (Euler et al., 2014). Cone bipolar cells are also named for their functional response to light turning on or off. ON and OFF bipolar cells depolarize in response to the onset and offset of light, respectively. The opposite responses to the same light stimulus stem from two different types of glutamate receptors. Bipolar cell types express either ionotropic and metabotropic glutamate receptors (iGluRs and mGluRs) (Wässle, 2004). Ionotropic

receptors, which form a complex with cation channels, open after binding glutamate, inducing hyperpolarization of the cell (Kolb et al., 2016). In contrast, metabotropic glutamate receptors that bind glutamate initiate a signal cascade to close cation channels, resulting in depolarization of the bipolar cell (Kolb et al., 2016). The separate glutamate receptors, in combination with selective wiring between bipolar cells and photoreceptors, allow bipolar cell types to parse the visual stimulus into distinct components. For example, the ON S-cone bipolar cell will depolarize in response to short-wavelength light turning on, but not in response to medium-wavelength light turning on or short-wavelength light turning off.

Bipolar cell somas sit within the inner nuclear layer and their axons terminate within the inner plexiform layer (IPL) of the retina (Figure 1). The inner plexiform layer can be broken into two layers: the ON and OFF layers, where ON and OFF bipolar cell axon terminals stratify, respectively (Figure 1) (Wässle, 2004). Ganglion cell dendrites also stratify in these layers and their stratification patterns typically predict their function (Wässle, 2004); ON, OFF and ON/OFF ganglion cell dendrites will terminate in the ON, OFF, or both ON and OFF layers, respectively. Ganglion cell somas sit below the IPL in the ganglion cell layer of the retina. Amacrine cells are the feedback neurons of the IPL and their cell bodies can be found within the inner nuclear layer, or within the ganglion cell layer. Amacrine cells are an extremely diverse group of cells (estimates vary but at least 40 types are suspected) and yet these cells are not well understood (Masland, 2012; Kolb et al., 2016). The star-burst amacrine cell received a lot of attention after it was found to be a key component in

circuitry responsible for motion detection in specific directions (Vaney et al., 2012). The AII amacrine cell is the most numerous and possibly the most studied amacrine cell (Demb and Singer, 2012; Kolb et al., 2016). Amacrine cell dendrites are dispersed throughout the ON and OFF layers of the IPL and provide inhibitory feedback onto bipolar cell axon terminals or directly onto ganglion cell dendrites.

The ganglion cells, which sit in the ganglion cell layer, are the output neurons of the retina. The functional properties of a ganglion cell are defined to a large degree by its pre-synaptic circuitry (Figure 2). A ganglion cell's receptive field, which is the area of the visual field that the cell is sensitive to, is dependent on the receptive fields of its pre-synaptic bipolar cells. The receptive field of a single bipolar cell is defined by the photoreceptors its afferents. Ganglion cells integrate the entirety of their pre-synaptic circuitry and this information is passed out of the eye along the optic track to the brain. Ganglion cell diversity is thought to surpass 30 cell types, each cell type representing a single parallel pathway (Sanes and Masland, 2014; Baden et al., 2016).

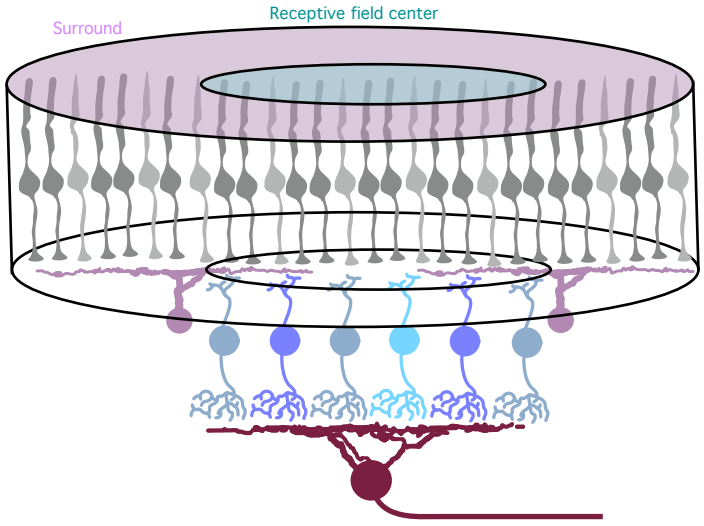

Figure 2. The functional properties of a ganglion cell are dependent on its inputs. Multiple bipolar cell types (blue-colored cells) contribute to a single ganglion cell (red). The bipolar cells' pre-synaptic photoreceptors (grays) make up the ganglion cells' receptive field center. Horizontal cells (pink) post-synaptic to surrounding photoreceptors provide inhibitory feedback to bipolar cells and create the surround of the receptive field, which has an opposite, but reduced, response to visual stimulus as the receptive field center. Adapted from (Dhande et al., 2015).

Parallel Pathways

The visual scene is filtered through the parallel pathways of the retina before being sent to the brain. Each ganglion cell type represents a separate visual pathway. Ganglion cells encode light increments and decrements, edge detection, color and even motion. To ensure that each parallel pathway can properly sample the entire visual scene, the receptive fields of a single ganglion cell type will tile the retina in a mosaic fashion, such that the entire visual field is sampled in a controlled manner (Figure 3) (Masland, 2012). The mosaic patterning of an individual ganglion cell type is independent of other ganglion cell types, such that mosaics of any two ganglion cell types are overlapping and not correlated (Figure 3) (Masland, 2012). This mosaic relationship is also true at the bipolar cell level. Bipolar cell types tile the retina and the receptive fields of individual types create mosaics to capture the entire visual scene (Figure 4) (Wässle et al., 2009; Euler et al., 2014).

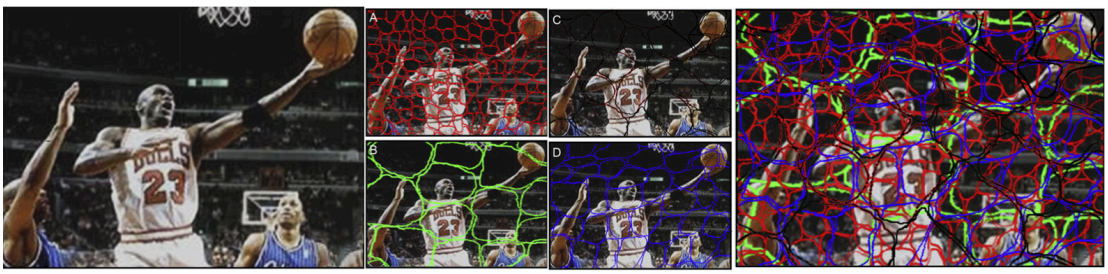

Figure 3. Ganglion cell receptive fields of the same cell type tile the retina in a mosaic fashion to sample the entire visual scene with little overlap to reduce redundancy.
Example mosaics in A, B, C, and D. Colored shapes represent the receptive fields of individual ganglion cells. Shapes of one color show the mosaic receptive field tiling of a single cell type. Shapes are packed together to sample the entire visual field with minimal overlap. Mosaics of different ganglion cell types overlap substantially. Adapted from (Masland, 2012).

The separate but overlapping (Figure 3) parallel pathways are only possible because of the selective synaptic wiring between retinal cell types. For example, in order for the rod pathway to reliably relay rod responses to ganglion cells rod bipolar cells must synapse almost exclusively with rod photoreceptors. Bipolar cells responsible for encoding color will synapse exclusively with either S- or M-cones. The mechanisms involved in this process are mostly unknown although a recent study looked at the diverse strategies across cone bipolar cell types used to develop and refine circuitry. (Dunn and Wong, 2012) showed that one type of bipolar cell in the developing retina expanded its dendritic tree towards its presynaptic partners and then stabilized while another type of bipolar cell overshot its targets before pruning its dendritic tree back to its adult resting state. The existence of these or similar mechanisms within the adult retina will be explored in this thesis.

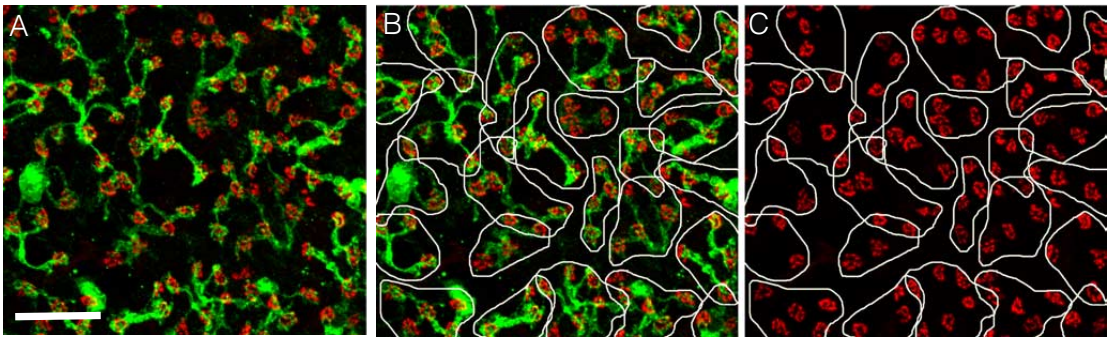

Figure 4. Dendritic territories of a single cone bipolar cell type in the mouse retina. A. Dendrites of Type 2 bipolar cells (green) synapse with cone pedicles (red). B. Contours outline individual dendritic territories. C. Cone pedicles are shown with just contours. Some cone pedicles are shared between bipolar cells. Scale bar 25µm. Adapted from (Wässle et al., 2009).

Motivation for the study of retinal plasticity

The healthy retina is a stable neural structure that only presents structural plasticity in response to injury or disease. This plastic response is typically known to be disruptive. Age-related macular degeneration (AMD), which results in photoreceptor cell death, is the leading cause of blindness in adults over 50 in the developed world (NEI, n.d.). Numerous inherited diseases result in retinitis pigmentosa (RP), a disease that causes photoreceptor cell death in younger people (affects 1 in 4000 people) (NEI, n.d.). Both AMD and RP cause photoreceptor cell death in the adult retina. Many of the changes in retinal structure and function following photoreceptor loss are conserved across different animal models of injury and disease (Marc et al., 2003). In response to injury (such as retinal detachment) or disease (such as photoreceptor degeneration), the bipolar cells and horizontal cells

send dendritic sprouts into the outer nuclear layer (ONL) often forming ectopic synapses (Strettoi and Pignatelli, 2000; Strettoi et al., 2003; Claes et al., 2004; Cuenca et al., 2004, 2005; Haverkamp et al., 2006; Michalakis et al., 2012). Bipolar cell axon terminals and amacrine cell dendritic processes atrophy (Claes et al., 2004; Cuenca et al., 2004, 2005; Barhoum et al., 2008; Lorach et al., 2015). Finally, retinal cells begin to displace out of their layers (Jones et al., 2003). The changes can be so drastic that in late stages of disease the retina becomes almost unrecognizable as cell somas move out of their retinal layers, disrupting the stereotyped structure and connectivity of the retina (Figure 5) (Jones et al., 2003).

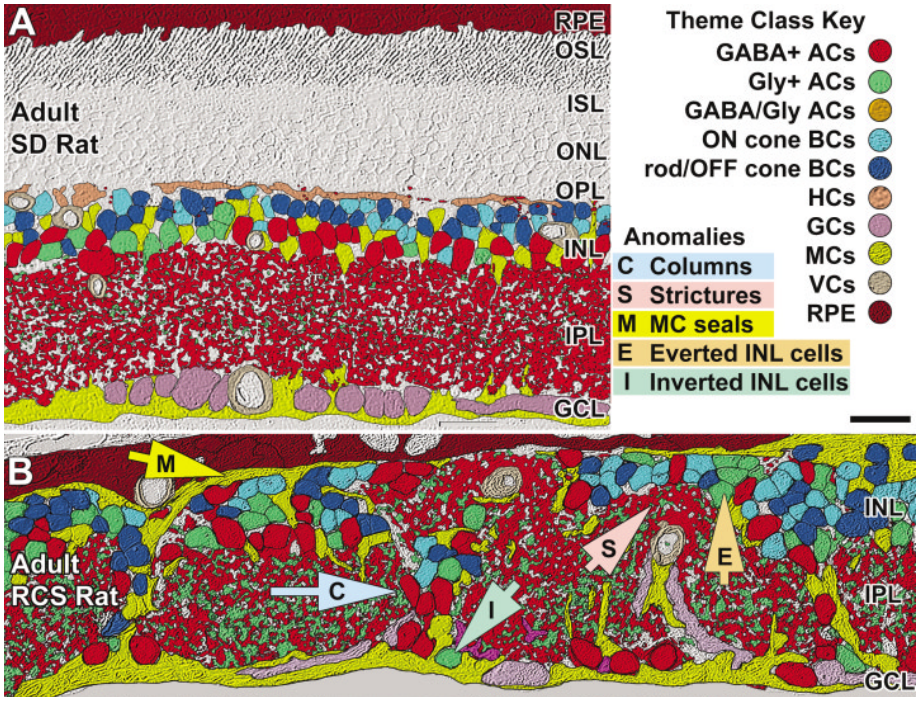

Figure 5. Retinal remodeling continues beyond the initial photoreceptor loss.

A. Retinal layers are clearly visible in a normal rat retina. B. In a rat degenerative retinal model, long after photoreceptor loss (+2 years), the remaining retinal layers are no longer recognizable. Arrows indicate specific anomalies. Cell types are abbreviated in the key as follows: Amacrine cells (ACs), bipolar cells (BCs), horizontal cells (HCs), ganglion cells (GCs), Muller cells (MCs), vascular cells (VCs), and retinal pigment epithelium (RPE). Many cells are displaced from their layers (e.g. an amacrine cell in the ganglion cell layer, marked by arrow labeled I). Adapted from (Jones et al., 2003).

Earlier in disease, plasticity mechanisms are less disruptive but still induce abnormal circuitry. In both a pig and mouse retinal degeneration models that experience rod photoreceptor loss, deafferented rod bipolar cells were found to synapse incorrectly with cones (Peng et al., 2000). Cone bipolar cells have also been reported to form incorrect synapses with rods after cone death (Haverkamp et al., 2006). In retinal disease models, photoreceptors die in a short period of time, leaving deafferented bipolar cells with limited alternative pre-synaptic partners. Can deafferented bipolar cells make new correct synapses if appropriate pre-synaptic partners are available? We find that correct synapse formation is possible in the adult retina and that these synapses are functional. The existence of these mechanisms in the adult retina is especially promising for the success of future therapies aiming to restore vision by replacing lost or malfunctioning photoreceptors with new photoreceptors that must integrate into the existing circuitry. Photoreceptor reintroduction therapies will only restore vision to degenerate retinas if the remaining circuitry rewires with the new photoreceptors.

This thesis work explores if, and the extent to which, bipolar cells in the adult retina can rewire with photoreceptors. Although we show deafferented bipolar cells

are capable of rewiring correctly with new afferents, we also find that different bipolar cell types use different wiring strategies and that the newly rewired circuits may not be as selective as developmental wiring mechanisms. The diversity of responses to deafferentation we see between bipolar cell types shows that different parallel pathways have access to different plasticity mechanisms, suggesting that they will respond to photoreceptor reintroduction therapies differently. A better understanding of the plasticity mechanisms available to the adult retina, and the diversity between parallel pathways, are integral in the pursuit of better vision restoration.

METHODS

Three methods are used continuously throughout this thesis and are described conceptually here. For each study, photoreceptors are ablated by selective photocoagulation, electrophysiology data is obtained using a multi-electrode array, and finally, histology data is collected from immunohistochemically treated retinas. The variations and technical parameters used within these methods are described within the sections unique to each study.

Selective Photocoagulation

Photocoagulation is a term used to describe the destruction of tissue using photons. In selective photocoagulation we control the volume of tissue destruction and localize the destruction to a particular area of interest. Throughout this thesis we selectively ablate photoreceptors to deafferent bipolar cells within a small patch of retina, leaving surrounding neurons intact.

An anesthetized animal's pupil is dilated and the back of the eye is viewed through a slit-lamp microscope such that the retina comes into focus. Once in focus, a short laser pulse is triggered. The laser light (532nm) passes through the retina, which is transparent to green light, and is absorbed by the pigmented epithelium at the back of the eye (Figure 6A). The resulting heat bubble destroys the surrounding tissue creating a lesion.

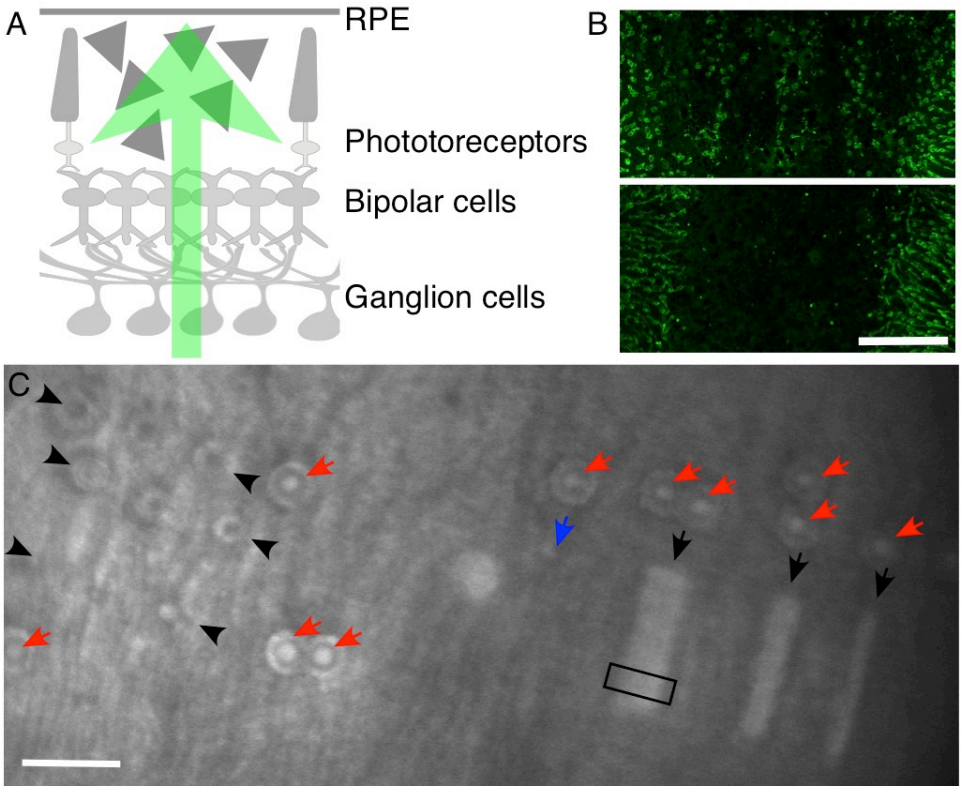

Figure 6. Selective photocoagulation *in vivo*.
A. A schematic showing laser light (green) traveling through the transparent layers of the retina until being absorbed by the pigmented epithelium (RPE). The heat bubble destroys photoreceptors, leaving the remaining retinal circuitry unharmed. B. Initial experiments placed line-scanned lesions side-by-side resulting in surviving photoreceptors between line scans (top panel). Overlapping the line scans by half the beam diameter eliminated surviving photoreceptors (bottom panel). Scale bar 100µm. C. Infrared bright field image of a rabbit retina *in vivo* immediately post lesion placement. Line lesions of different widths are visible as lighter gray areas where the RPE has been burned (black arrows). Spot lesions, titrated to destroy additional retinal layers, are placed close to experimental lesions to mark their placement and aid in locating them in the future (red arrows). A space has been left empty for a line lesion to be placed at a later date (blue arrow). Spot lesions were also placed in this retina for titration purposes and are visible in rows between the black arrowheads. A high-resolution image of the photoreceptor layer in the boxed area would resemble the panels shown in B. Scale bar 1mm.

The size of the ablation zone is dependent on three tunable parameters: laser beam diameter, laser power, and the amount of time the laser spends in the same area. Titration experiments determined the extent of tissue destruction at different laser settings. Larger areas of photoreceptor destruction were possible by scanning the laser in a line along the retina and placing multiple lesions next to one another. Early titration experiments showed that immediately adjacent lesions left surviving photoreceptors between line scans (Figure 6B). Overlapping scanned lines, instead of placing them immediately adjacent to one another, prevented photoreceptors from surviving in the lesion center (Figure 6B). Laser power and scan times are species dependent. A set of parameters that are known through titration experiments to destroy photoreceptors while leaving post-synaptic bipolar cells unharmed is used in experiments. The results from titration experiments are summarized in the following tables. Rabbit spot and line lesions are shown in Table 1 and Table 2, respectively. Spot and line lesions used in ground squirrel retinas are shown in Table 3 and Table 4, respectively.

Many photocoagulation lesions are placed in each eye of the animal. In some cases, space is left for lesions to be placed during future photocoagulation experiments such that lesions of different ages (ranging from 3 days to 4 months) can be directly compared within the same retina (Figure 6C). Retinas are harvested for functional and morphological experiments at predetermined time points after the photocoagulation procedure.

Beam diameter (μm)	Power (mW)	Pulse Duration (ms)	Rating
200	75-110*	20	Barely Visible
400	175-225	20	Barely Visible
200	250	50	Marker Burn

*The range of power settings typically used to achieve a Barely Visible spot burn. Ranges should be used as guidelines only. Spot lesions are titrated separately to each eye in each rabbit and can even require power adjustments based on location (peripheral retina vs. near optic streak).

Table 1. A summary of the laser settings used to produce spot lesions in rabbit retina. Typically, lesions were titrated in the superior rabbit retina and placed in the inferior retina for experiments. Laser settings were adjusted to the inferior retina if necessary. Marker burns were usually not titrated, although, if a burn resulted in a bleed the power was reduced.

Beam diameter (μm)	Power (mW)	Scan spacing (beam diameter)	Scan speed (m/s)	Iterations (applied at 10Hz)	Notes
100	1200	0	1.666	1	Barely Visible rating*
100	1500 1600	0	1.666	1	Visible rating
100	>1700	0	1.666	1	Very Visible rating. Maximum power setting of 2100mW** used for this rating.
100	2000	0	1.666	1	Photoreceptors survived between the line scans of larger (200 and 400μm wide) lesions.
100	2200	-0.5	1	2	The slower scan speeds resulted in less photoreceptor destruction***.
100	2000 2200	-0.5	1.666	2	Reduced the presence of surviving photoreceptors.

*Ratings normally applied to spot lesions were applied to line lesions here. Jennifer Kung placed and rated lesions. Spot and line lesions appeared to affect fundus whitening differently; lines looked stronger than spots due to a brighter and more immediate whitening of the RPE. These lesions were placed in an attempt to rate line lesions in a manner similar to spot lesions. The ratings, in the end, were not comparable. A Barely Visible line lesion did not destroy the photoreceptor layer (BV spot lesions do). This rating system was not used for future line lesions experiments.
**In another rabbit, 3000mW lines were used without an obvious increase in photocoagulation damage. Conversations with Daniel Palanker led to the conclusion that the laser power, regardless of software settings, could not be increased past ~2.4W.
***A rabbit with lines scanned at 1.0m/s and 1.666m/s and 2 iterations showed unexpected results. Slower scan speeds reduced photoreceptor destruction. This was not investigated further.

Table 2. A summary of the line lesion parameters used in rabbits.
Line lesions were not titrated to individual rabbits. Settings predetermined from the titration experiments summarized in the table were used for all rabbits and all areas of the retina. The length of the line lesions went unchanged throughout titration experiments at 1.5mm. Also, aim intensity and aim refresh were near 45% and 35Hz, respectively. These settings are set at the surgeon's preference. The aim settings do not affect the photocoagulation procedure but help the surgeon target the injury to a specific area of retina.

Beam diameter (μm)	Power (mW)	Pulse Duration (ms)	Rating
200	60-100	20	Barely Visible
400	145	20	Barely Visible
200	140	20	Marker Burn
100	200	50	Marker Burn

Table 3. A summary of the laser settings used to produce spot lesions in ground squirrel retina.
Spot lesions were quickly dropped in favor of line lesions in the ground squirrel retina. The extent of photoreceptor destruction for the Barely Visible lesions is unclear because the lesions could not be consistently found in immunostained retinas. A lack of damage could explain 'invisible' lesions although lesion misplacement in early experiments when lesions maps were still being improved could also explain the missing lesions. Line lesions (Table 4) were easier to locate and produced greater areas of damage.

Beam diameter (μm)	Power (mW)	Scan Spacing (beam diameter)	Scan speed (m/s)	Iterations (applied at 10Hz)	Notes
100	1300–1600	0	1.666	1	Lesions could not be easily located in immunostained retina.
100	1200 1300	-0.5	1.666	1	Not visible rating.
100	>1800	-0.5	1.666	1	Barely Visible to Visible ratings*. Maximum power 2400mW used.
100	1500–2400	-0.5	1	1	These settings produced fundus changes that best resembled lesions placed in rabbit retinas. Lesions placed with >1800mW destroyed photoreceptors completely.
100	2000	-0.5	1	1	Settings used for experiments.

*Ratings were graded by a different surgeon from line lesion grades in rabbit retina. Here, Seungjun Lee placed and graded line lesions.

Table 4. A summary of the line lesion parameters used in ground squirrels.
Line lesion lengths were all 1mm long. The curvature of the ground squirrel eye, and also the amount of retina visible through the slit lamp, prevented placement of longer lesions.

Electrophysiology

Electrophysiology is the study of neuronal activity. Here we use a multi-electrode array to detect the changes in voltage potentials that occur locally within the retinal tissue when a ganglion cell fires an action potential. The array allows us to detect these changes across a relatively large area of retina (1x2mm). By presenting the retina with a known stimulus and recording the ganglion cell responses, we can acquire the functional properties of individual ganglion cells. In a typical recording we identify hundreds of unique visually sensitive retinal ganglion cells.

Multi-electrode array

The multi-electrode array consists of 512 electrodes, spaced 60μm apart, embedded in a glass substrate. The retina, after removal from the eye cup, is placed retinal ganglion cell side down on top of the electrodes. The electrode array chamber is constantly perfused with an oxygenated solution that nourishes neurons. The retina can be kept alive and light responsive, *ex vivo*, for nearly 24 hours in this oxygenated solution. During a stimulus run, a stimulus movie played on a computer monitor is presented through the electrode array and retina and focused on the photoreceptor layer (Figure 7) (Litke et al., 2004). This orientation, light traveling through the

ganglion cell layer to the photoreceptors, matches the *in vivo* orientation. Furthermore, this orientation allows for our stimulus to be presented to retinal pieces that have been placed on the array with the pigment epithelium still attached. The pigment epithelium is a cell matrix that metabolically supports photoreceptors and in some species is required for a healthy electrophysiology experiment.

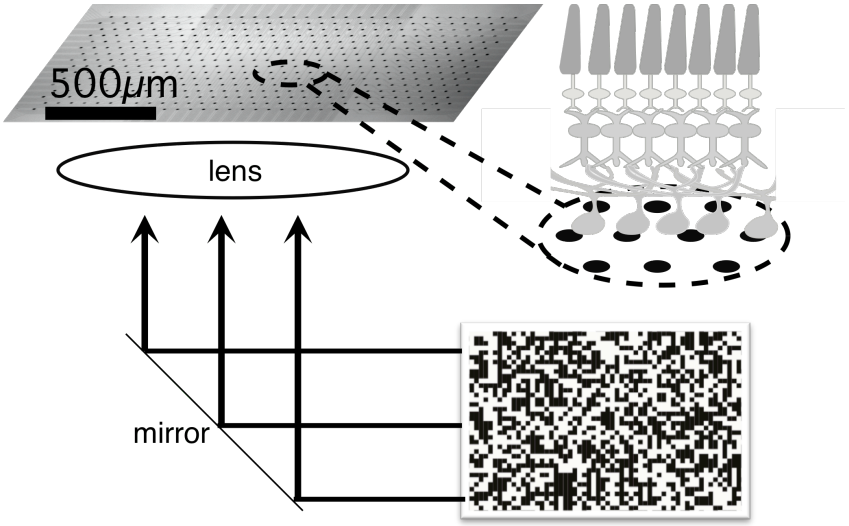

Figure 7. Electrophysiology experiment schematic.
A stimulus movie is focused through the multi-electrode array onto the photoreceptor layer of the retina, which is pressed ganglion cell-side down onto the array. The array sits in a perfusion chamber (not shown) that provides oxygenated Ames' solution to the tissue to keep the retinal neurons alive (*ex vivo*).

Stimulus

For this thesis, spatio-temporal white noise stimuli were used. Binary white noise stimulus is a movie of checkerboard-like images where each pixel flickers between black and white independently from all other pixels (depicted in Figure 7). Pixel size and the rate of flicker are controlled and set by experimental goals.

To detect color sensitivity within a retina a color noise stimulus is used. At each pixel red, green, and blue (RGB) are set to on or off independently of each other. Therefore, each pixel can flicker between black (RGB all off) and white (RGB all on) states as well as any RGB color combination in between.

Neuron Identification

Throughout a stimulus run, retinal ganglion cells are firing action potentials presumably in response to the stimulus. The local voltage changes on each electrode are recorded during the run. A typical stimulus run lasts 1-2 hours. After the experiment, the data is processed using a suite of custom software developed previously within the lab. The software automatically detects action potentials, assigns action potentials to neurons and calculates a neuron's spike-triggered-average.

Each electrode can detect action potentials from more than one ganglion cell and each ganglion cell's action potential can be detected on more than one electrode. Two steps take place to resolve this redundancy (Litke et al., 2004). First, action potentials at each electrode are assigned to individual neurons. Second, individual neurons are compared across electrodes to eliminate duplicates.

Action potentials are detected as a change in voltage above the noise at an electrode. Once an action potential is detected, the voltage trace is converted into a vector that can be projected into principle component space. In principle component space, action potentials are distributed by their greatest variance. Individual neurons have unique voltage signatures when firing an action potential. Therefore, action potentials can be clustered in principle component space by individual neuron. After

action potentials have been assigned to individual neurons at each electrode, a check for duplicated neurons is performed. The action potential trains found across electrodes are compared for timing correlations and highly correlated trains are removed.

Spike-triggered-average

The spike-triggered-average (STA) is named for its calculation: the average of the stimuli that elicited an action potential (Chichilnisky, 2001). For each neuron, a short movie clip of the stimulus presented to the retina just before each action potential is collected. All the collected movie clips from a single neuron are averaged together on a frame-by-frame basis such that you are left with the average movie clip presented just before an action potential (Figure 8A). This movie clip is the STA and provides spatio-temporal information about a neuron's response properties.

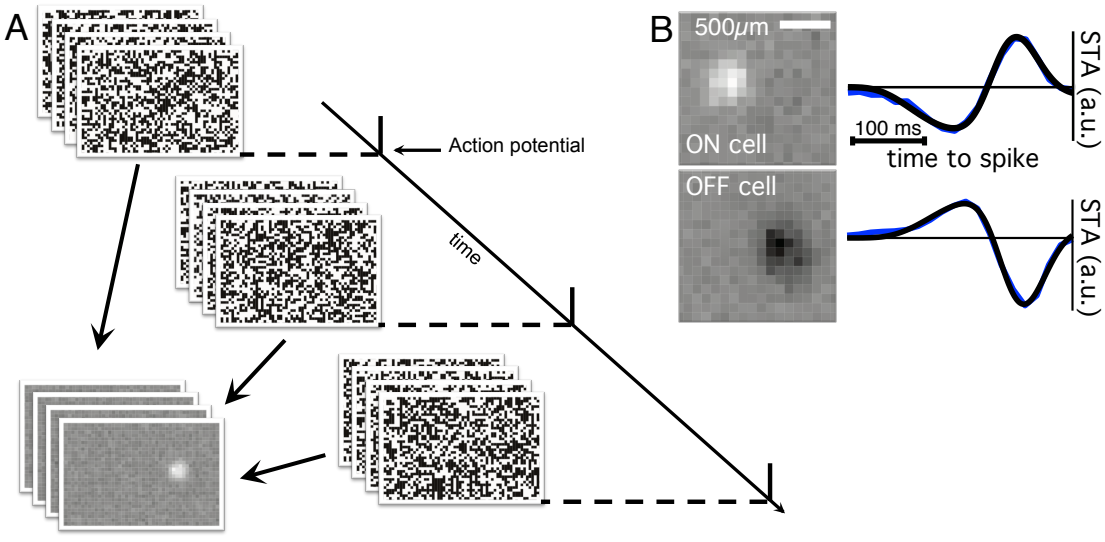

Figure 8. The spike-triggered-average of a ganglion cell.
A. Stimulus movie clips immediately prior to every action potential recorded of a single ganglion cell are collected and averaged frame-by-frame into a single movie clip. The averaged movie clip is the spike-triggered-average (STA) and gives the

spatial and temporal properties of the ganglion cell. B. The spatial property of a ganglion cell, its receptive field, is visible in a frame of the STA as non-gray pixels. The time course of the STA, an average of the luminance over time within a cell's receptive field, displays the temporal properties of a ganglion cell. An example ON and OFF ganglion cell are shown in the top and bottom panel, respectively.

The receptive field is the area of the visual scene that a ganglion cell is responsive to and describes the spatial properties of a ganglion cell. The receptive field of a ganglion cell is readily visible in a STA as the non-gray pixels. The size of the receptive field is dependent on the ganglion cell type and is one of the features that can be used to group functionally homogeneous ganglion cells together. Stimulus pixel size determines the resolution of the resolved receptive field. Smaller stimulus pixels can resolve a receptive field in more detail; however, larger pixels stimulate neurons better than small pixels. During an electrophysiological recording, stimulus pixel size is decided by balancing experimental goals with retinal response.

The temporal properties of a ganglion cell are given by the time course, which is the STA luminance within a cell's receptive field over time (Figure 8B) (Chichilnisky, 2001). This feature is unique between functional ganglion cell types. The stimulus frequency determines the resolution of the time course. Faster stimulus frequencies can describe a temporal response in great detail but do not drive neurons as well as slower frequencies. Typically, slower stimulus frequencies were chosen to help drive neurons with smaller stimulus pixels because, within this thesis, spatial resolution was of greater importance than temporal resolution.

Functional classification of retinal ganglion cells

Retinal ganglion cell types can be identified, and classified, by their spatio-temporal response properties to visual stimulus. During a stimulus run many types of ganglion cells are detected on the array. Afterwards, we attempt to group the neurons in to classes by cell type. Neurons are projected into principle component space by receptive field size calculated from the STA, the temporal aspects of the STA within a cell's receptive field and the autocorrelation between action potentials. Clusters of neurons are selected by hand and then checked for accuracy. A grouping of correctly classified cells will display a mosaic of receptive fields: non-overlapping receptive fields but complete coverage across the retina (Figure 9) (Litke et al., 2004). The functional properties used to classify the ganglion cells, such as the STA time course and autocorrelation function, show relative homogeneity as well (Figure 9).

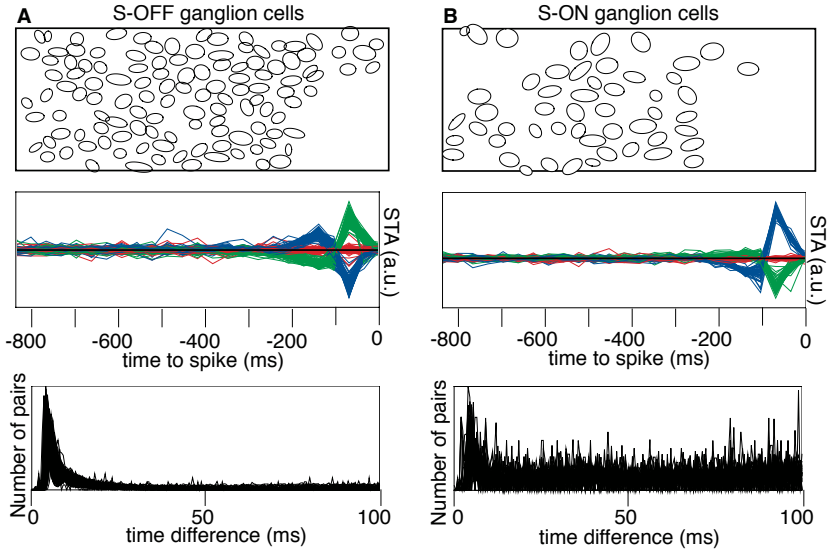

Figure 9. The functional classification of ganglion cells in a single retina.
A. A group of ganglion cells have been clustered together based on their receptive field size (ellipse size in top panel), their STA time course (middle panel), and their autocorrelation function (bottom panel). The receptive fields of the individual

ganglion cells (ellipses in top panel) do not overlap and tile the space suggesting a single cell type has been correctly identified. The time course (middle panel) and autocorrelation (bottom panel) show individual traces for each cell. The cell type is named for its temporal filter, which responds to blue light turning off and green light turning on within a cell's receptive field: S-OFF (M-ON) ganglion cell. B. Same as in A except for a different cell type within the same retina. This cell type is also named for its temporal filter: S-ON ganglion cell.

Histology

Histology is the study of tissue structure. We use immunohistochemistry to selectively label structures within the retina tissue such that we can study its morphology. Immunohistochemistry allows us to identify a variety of structures ranging from entire neurons to individual synapses. By looking at retinal tissue after photocoagulation we can study the structural changes within the tissue in response to photoreceptor ablation. This technique is also applied to retinal pieces that were used for electrophysiological recordings, thereby allowing us to directly compare functional and morphological data within the same retinal piece.

Immunohistochemistry

Immunohistochemistry makes use of antibodies, which are designed to bind specifically to proteins of interest. The retinal tissue is first fixed, which kills and preserves the tissue by forming covalent chemical bonds between proteins within the tissue. Next the tissue is treated with a protein-rich soapy solution. The protein-rich solution helps prevent non-specific binding in upcoming steps and the soap creates small holes within the tissue by removing the cell membrane lipid layers to allow for better diffusion. A primary antibody solution is applied to the tissue to bind the

protein of interest. Then, a secondary antibody, which is tagged with a fluorophore, is applied to bind the primary antibody. In this way, a protein of interest can be labeled with a fluorescent tag. Multiple (3-5) proteins of interest can be labeled, and later distinguished, within one piece of tissue.

The proteins of interest used here are known, in the literature, to label retinal structures relevant to this thesis. It is important to note that sometimes the protein of interest is only of interest because it is localized to specific structures. For example, staining for protein kinase C-alpha (PKCα) clearly labels the entire dendritic and axonal trees of rod bipolar cells. However, PKCα is not itself relevant to this thesis.

Image Acquisition and Analysis

Immunohistochemically treated retinas are imaged on a scanning laser confocal microscope. A 3D image of the stained structures in the retinal tissue is created by locally exciting fluorophores and scanning over a volume. Multiple fluorescent tags can be distinguished based on their excitation and emission spectrums. The Z-stack images are viewed in Fiji, a free image processing suite of software made available by the National Institutes of Health. Typically, initial image analyses are performed in Fiji and the results are then uploaded to custom MATLAB scripts to perform further calculations. Initial analyses consisted of collected data like cell body location measurements, dendritic projection angles, to creating binary image masks from image data. Analyses performed within MATLAB built upon data taken in Fiji. For example, I created scripts to calculate the relative angles of dendritic

projections to a lesion edge as well as scripts that used image masks to create region of interest boundaries in the 3D space.

RESULTS

Constructive plasticity exists in the adult retina

The analyses that I present in the following section have been published (Sher et al., 2013) and are my own, however, the experiments that produced the data I analyzed took place before I joined the project. I analyzed functional data from photocoagulated retinas. These analyses helped steer the main focus of my PhD thesis work and will also provide an introduction to the questions I will answer later in my thesis.

Introduction

Normally, the adult mammalian retina is a stable neural network, but it exhibits structural and synaptic plasticity in response to loss of photoreceptors during injury or disease. Typically, the resulting deafferentation of the inner retinal neurons disturbs the organized retinal structure, leading to abnormal circuit connectivity and function (Marc et al., 2003; Stasheff et al., 2011; D'Orazi et al., 2014). However, at the time the following experiments took place it was known that after local photoreceptor loss in the adult retina, neighboring photoreceptors would shift into the ablation zone (Paulus et al., 2008). The functional capabilities of the shifting photoreceptors was as yet unknown.

To investigate the functional consequences of local photoreceptor loss and the shifting photoreceptors Sher et al used the multi-electrode array to assess the visual

sensitivity of retina that had previously undergone photocoagulation therapy. Furthermore, (Sher et al., 2013), using computational molecular phenotyping, investigated the functional consequences to the inner retinal circuitry. We find that shifting photoreceptors are functional and will rewire with the deafferented bipolar cells at the lesion center, returning visual sensitivity to bipolar and ganglion cells. These findings show that constructive functional plasticity exists in the mammalian adult retina.

Methods

Photocoagulation

Laser photocoagulation burns were placed with the PASCAL laser system (Topcon Medical Laser Systems) using 532 nm light. Laser power was titrated to produce Barely Visible grade spot lesions, a clinically relevant grade defined as a faint but clearly visible lightening of the fundus pigmentation within 1 minute of laser therapy. The power range for 200μm spot size was 60–90mW with 20ms pulse duration. Thirty-seven male Dutch Belted rabbits (weight 2–3 kg) were used in accordance with the Association for Research in Vision and Ophthalmology Statement Regarding the Use of Animals in Ophthalmic and Vision Research after approval from the Stanford University Animal Institutional Review Board. 15 minutes prior to the photocoagulation procedure, the rabbits were anesthetized with ketamine hydrochloride (35 mg ketamine hydrochloride / kg of rabbit, injected

intramuscularly), xylazine (5 mg/kg), and glycopyrrolate (0.1 mg/kg). Pupillary dilation was achieved by 1 drop each of 1% tropicamide and 2.5% phenylephrine hydrochloride. Tetracaine 0.5%, a topical anesthetic, was applied to the eye before the treatment.

Electrophysiology

Eyes with photocoagulation lesions were enucleated under terminal anesthesia in dim red light. A 4x4mm^2 piece of retina with 2–3 lesions was isolated from the vitreous, and peeled away from the sclera and choroid. The retinal piece was placed on the electrode array and perfused with oxygenated Ames' solution, pH 7.4, and kept at 30°C. Visual stimulus (black and white binary spatiotemporal white noise, checker size 80μm, flicker frequency 60Hz) was presented to the retina. After the experiment, the retina was photographed on the array, with the position of the visual stimulus to enable aligning retinal ganglion cell spatial sensitivity profiles with lesion locations. Lesions were visible as hypopigmented spots on the retina and were verified against the known pattern of lesions. RGCs were characterized by their spike-triggered average (STA). For each identified RGC, the receptive field was outlined by its isosensitivity contour.

Computational Molecular Phenotyping with AGB

Computational molecular phenotyping (CMP, (Marc and Jones, 2002)) is a technique that identifies cell types based on the ratio of small molecules present in their cell bodies (see (Sher et al., 2013) for complete Methods). Another small

molecule, 1-amino-4-guanidobutane (AGB) is known to enter active (firing) neurons. Cell types in lesioned retina exposed to light flashes were identified with CMP and, in combination with AGB, were evaluated for their responsivity to light. AGB levels within a cell were calculated as the average illumination within a cell body of a gray-scale image. Cells outside a 2 day old and a 2 month old were used to normalize each cell type.

Response properties of RGCs

Visual sensitivity was calculated as the sum of STA responses of RGCs inside the lesion and normalized to STA responses outside the lesion. Visual sensitivity calculations for ON and OFF pathways were calculated by separating ON and OFF RGCs and recalculating the visual sensitivity of each group.

Response kinetics of individual ganglion cells were broken down into STA kinetics inside and outside of the ablation zone. Time to peak, time to zero and the degree of transiency were calculated from time course measurements from inside the lesion and outside the lesion fitted separately to the function:

$$\text{fit} = \text{a}\left(\frac{t}{c}\right)^{e} * \exp\left(-\text{e}\left(\left(\frac{t}{c}\right)-1\right)\right) - \text{b}\left(\frac{t}{d}\right)^{f} * \exp\left(-\text{f}\left(\left(\frac{t}{d}\right)-1\right)\right),$$

where constants a–f were solved for using a non-linear least squares fit routine in MATLAB. The degree of transiency was defined as $1 - |\int time\ course| / \int |time\ course|$. For data on 'false' lesions, an area equivalent in size to a lesion was placed randomly within an area of unlesioned retina and the same previous calculations were repeated.

Results

Visual sensitivity returns to the retina after photoreceptor ablation

Adult rabbits were treated with Barely Visible grade burns using a 200µm beam diameter to destroy a small patch of photoreceptors, leaving inner retinal neurons intact. Immediately after photoreceptor ablation, there was a blind spot within the lesion, as expected (Figure 10A). Surprisingly, after 2 months the blind spot would disappear as photoreceptors filled into the lesion (Figure 10A). Visual sensitivity returned to both ON and OFF retinal ganglion cell classes within 2 months ($p>0.07$, Figure 10B).

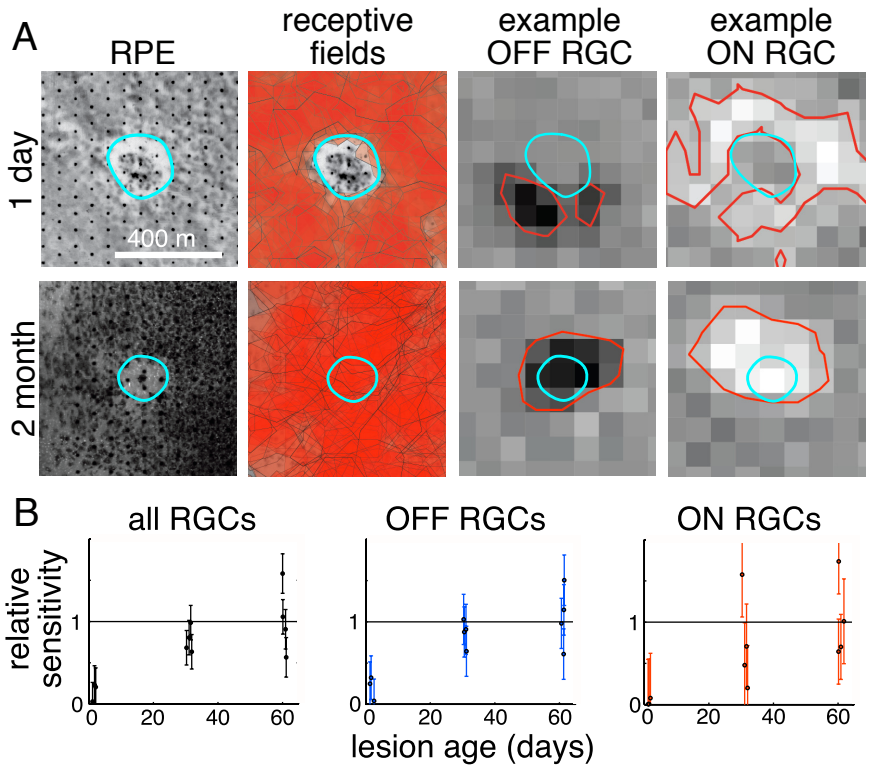

Figure 10. Blind spots created by selective photocoagulation of the photoreceptors disappear in 2 months.
A. Retinas with 1-day-old and 2-month-old lesions are imaged on the array (regular grid visible through 1-day-old retina) to locate the lesions, visible as a change in pigmentation of the retinal pigment epithelium (RPE). Cyan contour outlines the single lesion in the field of view for all panels. Receptive fields of all identified retinal ganglion cells (RGCs) are overlaid on the RPE image. Receptive fields completely overlap with the ablation zone 2 months after the ablation. Spike-triggered average frames and receptive fields (red contours) of example individual ON and OFF RGCs. Blind spots are visible in receptive fields of individual cells 1 day post-ablation. 2 months post-ablation, receptive fields of individual cells fill into the blind spot. B. The relative visual sensitivity of all RGCs returns to normal 2 months post-ablation. When split into functional classes, both ON and OFF RGC types show a return in visual sensitivity. Adapted from (Sher et al., 2013).

To determine if the restored vision was normal or altered due to the injury, I compared the response kinetics of ganglion cells' receptive fields within and without the lesion space. Within each preparation, a population of ganglion cells had receptive fields that overlapped with the original lesion space (Figure 10A). Normally, a ganglion cell is characterized by its STA time course. The significant STA pixels define a cell's receptive field. To compare the response properties of lesioned and unlesioned retina, I separated individual ganglion cell receptive fields into two parts: STA pixels outside or inside the lesion (Figure 11A).

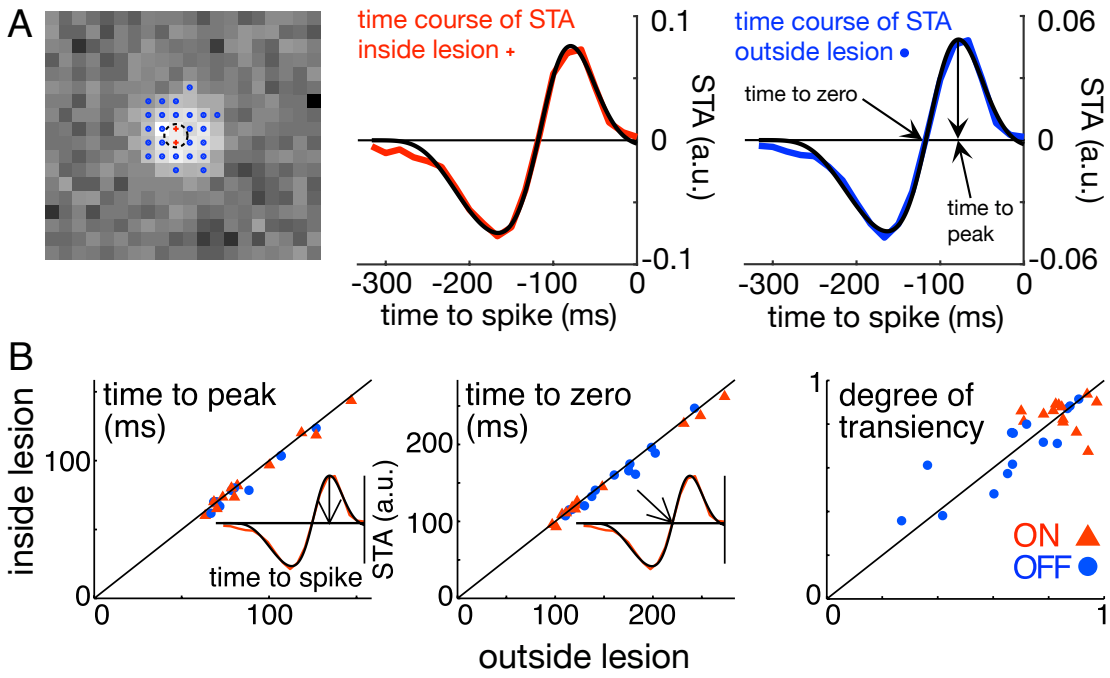

Figure 11. The response kinetics of ganglion cells with receptive fields that overlap the ablation zone.
A. An example ON ganglion cell STA frame is marked to denote the original ablation zone (dashed circle) and the pixels within the receptive field defined as inside the ablation zone (red crosses) and outside the ablation zone (blue dots). The time course of the STA is then measured separately for inside (red line) and outside (blue line) the ablation zone and fitted separately (smooth black lines). B. Three time course response kinetics, calculated from the fitted data, are compared between inside and outside the lesion: time to zero, time to peak and degree of transiency (defined as 1-abs(integral time course)/integral(abs(time course)).). n = 27 retinal ganglion cells in 4 2-month-old lesions across two retinal preparations. Adapted from (Sher et al., 2013).

I then fitted time courses to the inside and outside of the receptive fields separately. I compared three kinetic traits between the inside and outside time courses that are known to be sensitive to the circuitry within the retina and are also commonly used to classify functional ganglion cells: time to peak, time to zero, and degree of transiency. I found no difference in retinal ganglion cells' response to visual stimulus inside or outside a lesion (Figure 11B). I did the same analysis to areas of healthy retina where

I designated a false lesion and also found no difference in the response kinetics (Figure 12). Therefore, the returned visual sensitivity after selective photoreceptor ablation appears normal.

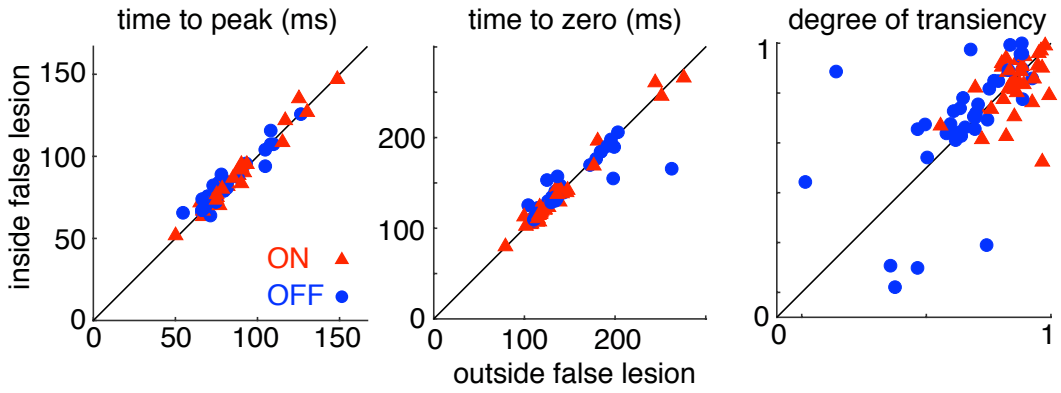

Figure 12. The response kinetics of ganglion cells with receptive fields that overlap a false ablation zone.
Same as Figure 11B except within healthy retina. An area of healthy retina, equal in size to the ablation zone in Figure 11, was designated as a false ablation zone. Response kinetics, as described in Figure 11, were compared between inside and outside the false ablation zone. n = 79 retinal ganglion cells in 8 false lesions across 2 retinal preparations.

Deafferented bipolar cells regain light sensitivity after photoreceptor ablation

One of three mechanisms could lead to vision restoration within the lesion space. Either, photoreceptors shift into the lesioned space, maintaining their original connections, or, photoreceptors could shift into the lesioned space and rewire with the deafferented bipolar cells within the lesion (Figure 13). The third mechanism combines the first two; shifting photoreceptors make new post-synaptic partners while maintaining old post-synaptic partners.

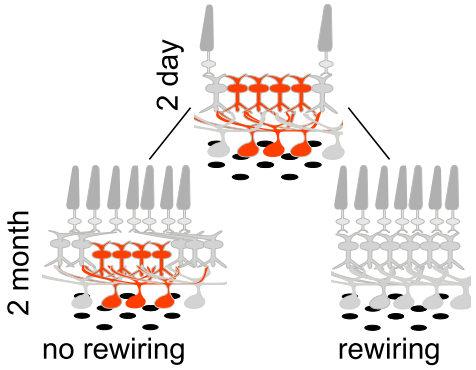

Figure 13. Mechanisms for vision restoration after local photoreceptor ablation. 2 days post ablation, bipolar cells are deafferented and not visually sensitive (red). Retinal ganglion cells post-synaptic to deafferented bipolar cells also lose visual sensitivity in the ablation zone. After 2 months, surrounding photoreceptors shift into the ablation zone and either bring their original post-synaptic partners with them, leaving the deafferented bipolar cells visual insensitive (no rewiring), or the shifting photoreceptors will make new connections with the deafferented bipolar cells causing them to regain visual sensitivity (rewiring). A third mechanism for vision restoration, not depicted, is a combination of the two depicted mechanisms. Adapted from (Sher et al., 2013).

To distinguish between these mechanisms, Sher et al performed computational molecular phenotyping (CMP) on acute and older lesioned retina in combination with 1-amino-4-guanidobutane (AGB) labeling to detect neural activity. CMP classifies retinal cell types based on their metabolic mechanisms by detecting the ratios of small molecules within a cell body. AGB is a small molecule that only enters a neuron when it is active, for example, in response to light flashes. Lesioned retina was analyzed for neural activity on a cell-by-cell basis by exposing it to light flashes and AGB *in vivo* and combining AGB labeling and CMP techniques. After (Sher et al., 2013) identified the cell types within the lesioned retina using CMP (Figure 14A), I segregated the cells within and without the lesion (Figure 14B,C). I noticed an increase in the number of bipolar cells inside the 2 month old lesion (Figure 14C). We

did not have an explanation for this increase at the time of these experiments, except that neurogenesis was not the cause. In the next section within this thesis, we present evidence that the increase in bipolar cells is likely due to wound contraction, causing the tissue to shrink and increase cell density inside the ablation zone. After segregating cell types based on being inside or outside the ablation zone I then compared AGB levels inside relative to levels outside the ablation zone (Figure 14D). Cells within 2-day-old lesions had reduced AGB levels, indicating reduced neural responses to flashes of light. However, cells within a 2-month-old lesion regained normal AGB levels indicating a return of visual sensitivity (Figure 14D). Only GABAergic amacrine cells showed a decrease in relative AGB levels between 2-day and 2-month-old ablation zones and we cannot explain why. The wide dendritic fields of the amacrine cells may protect them from drastic changes in their visual sensitivity after the loss of a small portion of their dendritic field. However, the decrease in visual sensitivity is unexpected in relation to the increase AGB levels in the other cell types. The observed decrease could be related to retinal restructuring or a statistical outlier. I did not look at AGB levels in horizontal cells due to the small sample size. The return of visual sensitivity to deafferented bipolar cells, both ON and OFF types, lead us to conclude that the shifting photoreceptors are making new synaptic contacts with the deafferented bipolar cells.

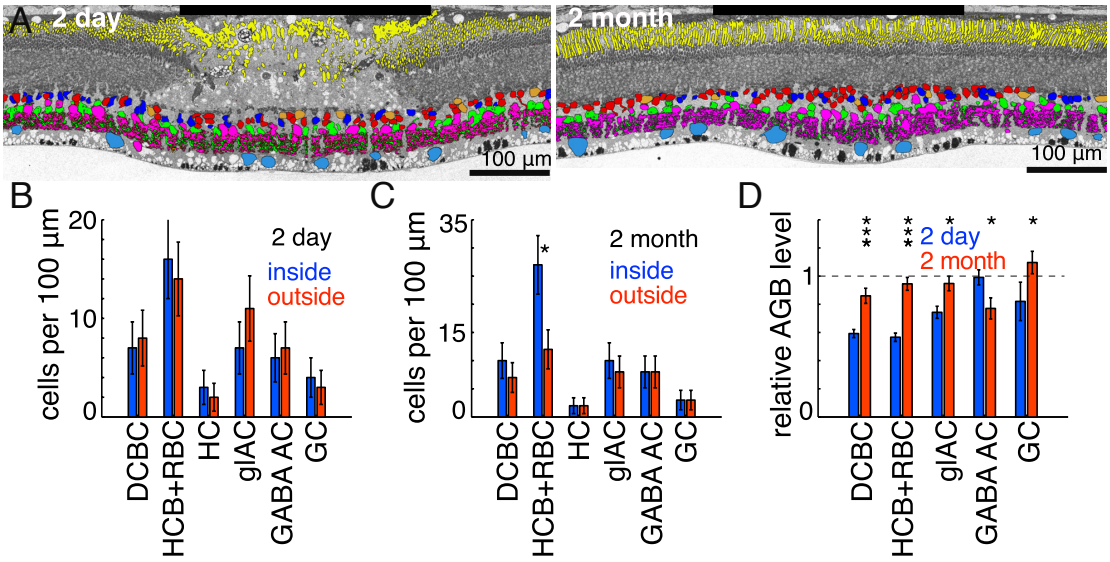

Figure 14. Visual sensitivity by cell type within an acute and older ablation zone. A. Retina sections through a 2-day-old and 2-month-old ablation zone with cell types identified by computational molecular phenotyping overlaid in pseudocolors. Cell type pseudocolors: horizontal cells are orange, hyperpolarizing cone bipolar and depolarizing rod bipolar cells are red, depolarizing cone bipolar cells are dark blue, GABAergic amacrine cells are magenta, glycinergic amacrine cells are green, ganglion cells are light blue, and rod outer segments (identified with rhodopsin) are yellow. Black bar indicates width of ablation zone. B. The density of cells (cells/length), broken down by cell type, inside and outside the 2-day-old ablation zone. Cells per 100µm +- $n^{1/2}$. C. The density of cells inside and outside the 2-month-old ablation zone. Cells per 100µm +- $n^{1/2}$. D. The average amount of AGB within the cells inside the 2-day and 2-month-old ablation zone, broken down by cell type. Averages are normalized to average cell type AGB levels outside the ablation zone. Mean +- SEM. *p<0.05, and ***p<0.001. Adapted from (Sher et al., 2013).

Discussion

The (Sher et al., 2013) study showed that the adult retina is capable of synaptogenesis between photoreceptors and bipolar cells and that the new synapses are functional. This functional plasticity is present in both the ON and OFF parallel pathways of the retina.

Two major questions were raised by this study. First, can all bipolar cell types within the adult retina rewire with new photoreceptors? The current study is limited in its classification of bipolar cell types to two broad categories: ON and OFF bipolar cells. There are about half a dozen functionally and morphological distinct bipolar cell types within both the ON and OFF classes. For example, rod bipolar cells, which are canonically part of a separate parallel pathway, are indistinguishable from cone ON bipolar cells in this study. As a population, both ON and OFF bipolar cells regain visual sensitivity, however, it remains unknown if individual cell types within these populations differ in their ability to rewire.

The second question this study leaves unanswered is, what are the mechanisms behind the synaptogenesis? The term mechanism here is purposefully broad. There are, almost certainly, many mechanisms involved in synaptogenesis that range from molecular mechanisms within the cell that control synapse formation to structural plasticity mechanisms that allow the cell to change its dendritic tree. In the course of my thesis, I will focus on discovering the structural mechanisms that allow for dendritic tree changes and explore how these mechanisms differ across bipolar cell types.

Deafferented adult rod bipolar cells create new synapses with photoreceptors to restore vision

In the effort to investigate how bipolar cells in the adult retina regained visual sensitivity after local photoreceptor loss I used immunohistochemistry to look at known inner nuclear layer cell types in the rabbit retina. During preliminary experiments I also switched from ablating photoreceptors in a small spot to line-shaped ablation areas. The high aspect ratio of line-shaped lesions allowed me to study lesion dynamics on a larger scale without causing a deeper photocoagulation burn. To ensure that both spot and line lesions had similar healing dynamics I confirmed that photoreceptors shifted into the ablation zone of line-shaped lesions. Early immunohistochemistry experiments suggested that rod bipolar cells were extremely plastic in response to local photoreceptor ablation. Therefore, for the functional characterization of the lesioned retina, I pursued electrophysiology experiments at scotopic (rod) light levels in addition to the photopic (cone) functional characterizations. The following sections, excluding edits for clarity, have been published (Beier et al. 2017).

Introduction

Previous studies have shown that not all changes in the retina after injury are disruptive. In particular, local and selective ablation of photoreceptors leads to the shift of the surrounding healthy photoreceptors into the lesioned area (Busch et al., 1999; Paulus et al., 2008; Lavinsky et al., 2013; Strazzeri et al., 2014). Furthermore, it

was shown that the shifting photoreceptors provide inputs to the retinal circuitry and that the inner retinal neurons in the lesioned area become responsive to light (Sher et al., 2013). However, it is unclear how the shifting photoreceptors integrate into the deafferented portion of the retina, and if the new connectivity is similar to that in the healthy retina. One approach to restore vision in patients blinded by the loss of photoreceptors is based on the reintroduction of healthy photoreceptors into diseased retina (MacLaren et al., 2006; Singh and MacLaren, 2011; Pearson, 2014). The success of this approach depends on the ability of the remaining retinal cells to form new synapses with the introduced photoreceptors, while maintaining normal connectivity patterns in the inner retina.

We use short-pulse laser photocoagulation to selectively ablate a patch of photoreceptors in adult rabbits, leaving the bipolar cells intact but deafferented. Using immunohistochemistry to visualize the photoreceptor and bipolar cells at different times after ablation and multi-electrode array recordings to monitor visual function, we find that the adult rabbit retina is capable of synaptogenesis, while avoiding some of the deleterious structural changes associated with retinal degeneration. We observed dramatic morphological rearrangement of the dendrites from rod bipolar cells, resulting in their targeted expansion toward healthy photoreceptors. Extended rod bipolar cell dendrites make synaptic contacts with new rod afferents, and thereby restore vision in the adult mammalian retina.

Methods

Selective Photocoagulation

Adult Dutch Belted rabbits were used in accordance with the Association for Research in Vision and Ophthalmology Statement Regarding the Use of Animals in Ophthalmic and Vision Research after approval from the Stanford University Animal Institutional Review Board. Rabbits, of either sex, were anesthetized using ketamine hydrochloride (35mg/kg rabbit, IM) and xylazine (5mg/kg rabbit, IM) 15 minutes before the procedure. A single drop of both 1% tropicamide and 2.5% phenylephrine hydrochloride was applied to each eye to dilate the pupil. Lesions were applied to the retina with a scanning laser (PASCAL, 532nm) using a custom scanning software. A laser beam of 100µm in diameter was scanned twice with 100ms delay over 1.5mm length of the retina at 1.6m/s scanning velocity and power of 2.0 - 2.2W. Laser settings were titrated in preliminary experiments that checked for photoreceptor destruction with immunohistochemistry. Line lesions, unlike barely visible clinical grade spot lesions, showed an immediate whitening of the fundus when placed, in vivo, in rabbit retinas. Lesions of 200µm and 300µm in width were created by overlapping multiple 100µm-wide scans, such that the overlap was equal to half the beam diameter. Therefore, a 200µm-wide lesion was made with 3 overlapping 100µm-wide lines, and a 300µm-wide lesion required 5 lines. Rabbits underwent this procedure twice in order to place acute (3-16 day old) lesions near (~400µm from) older (1-4 month old) lesions.

Electrophysiology and Analysis

Lesioned eyes were enucleated under terminal anesthesia in dim red light. The anterior portion of the eye, the lens, and the vitreous were removed from the eye cup. The eye cup, with retina still attached to RPE and choroid, was kept in oxygenated Ames' solution (Sigma-Aldrich) heated to 32°C and kept in the dark, except to remove pieces of retina for placement on the array. A 4x4mm piece of retina containing 4 lesions (two acute and two older lesions) was isolated from the choroid under an infrared microscope and placed ganglion cell side down onto the array (1.7 mm^2 area) such that 2-3 lesions overlapped with the electrodes. Peanut agglutinin (PNA) 568nm (1:100 in Ames, Life Technologies) was added to the array chamber before the retina piece was oriented on the array. During the experiment, the retina was perfused with fresh oxygenated Ames' at 32.4°C. Stimuli were presented to the retina by a CRT computer monitor focused through the microscope objective onto the photoreceptor layer. After presenting stimuli, we imaged the relative positions of the array and stimulus, as well as the photoreceptor outer segments (visualized with PNA), so that we could map lesion locations to the presented stimulus. For scotopic recordings, retinal pieces were dissected using only infrared illumination. The retina was then presented a light stimulus at 5-12 Rhod*/rod/sec, using neutral density filters to reduce the light intensity. To obtain rod-light levels, either 3.0 or 2.6 neutral density filters (NDs) were placed in the optical path to reduce the amount of light reaching the array. Low light, (3.0 ND, equivalent to 5 Rhod*/rod/sec) was attempted first and if the retina was not responsive to visual stimulus, then the amount of light

was increased (2.6 ND, equivalent to 12 Rhod*/rod/sec). A photopic stimulus (3700 Rhod*/rod/sec) was presented immediately afterwards to provide direct comparison of a scotopic and photopic response from the same retinal preparation.

Photoisomerizations were calculated as follows:

Power meter measurement:

$$Amps_{measured}\ [A] = R\ [W] \cdot \sum^{\lambda} Calibration(\lambda)\ \left[\frac{A}{W}\right] \cdot CRTnormspectrum(\lambda)$$

Solve for unknown constant, R, and calulate $Power(\lambda)$.

$$Power(\lambda)\ [W] = R\ [W] \cdot CRTnormspectrum(\lambda)]$$

Calculate the number of photons, as a function of λ, to reach the multi-electrode array.

$$PhotonFlux(\lambda)\ \left[\frac{photons}{s \cdot \mu m^2}\right] = Power(\lambda)\ \left[\frac{J}{s}\right] \cdot \frac{\lambda}{hc}\ \left[\frac{photon}{J}\right] \cdot \frac{1}{spotsize}\ \left[\frac{1}{\mu m^2}\right]$$

Determine the number of photons available to rod photoreceptors across the array.

$$PhotonsAbsorbed\ \left[\frac{photons}{s \cdot \mu m^2}\right] = \sum^{\lambda} PhotonFlux(\lambda) \cdot RhodopsinAbsorption(\lambda)$$

Calculate the number of absorption events, per rod, that result in photoisomerization.

$$Photoisomerizations\ [^*Rhod/s/rod] = PhotonsAbsorbed \cdot q_{efficiency} \cdot \frac{radius_{rod}^2 \cdot \pi}{rod}$$

The *Calibration*(λ) function was obtained from the power meter manual, using the calibration curves for the meter without the attenuator (the measurement was taken without the attenuator). The CRT computer monitor spectrum, *CRTnormspectrum*(λ), was normalized such that its integral equaled 1. The energy of a photon as a function of wavelength, E(λ) = λ/hc, and the amount of light reaching the array, the spot size, was used to calculate the photon flux. The absorption spectrum of rhodopsin, with a peak absorption at λ = 500 nm, was used to determine the number of photons available to rod photoreceptors to reach the array. Photons are only converted into

photoisomerization events at a rate of quantum efficiency ($q_{efficiency}$) = 0.67 [Rhod*/photon].

After the experiment, the retina was removed from the array and prepared for immunohistochemistry.

Typically, spike trains of hundreds of individual retinal ganglion cells were identified from a single piece of retina using custom software that distinguishes action-potentials of individual cells through the unique voltage signals recorded on the electrodes (Litke et al., 2004; Field et al., 2007; Sher and Devries, 2012). Retinal ganglion cells were characterized by their spike-triggered average (STA) response to binary white noise stimulus (checkerboard-like stimulus: 45µm or 90µm checkers, flickering independently at 20Hz, 30Hz or 60Hz). Retinal sensitivity over space was calculated by adding the STA spatial sensitivity profiles of all the detected RGCs that had a 2.7 signal to noise ratio in their STAs.

Immunohistochemistry

Pieces of retinal tissue were separated from the choroid and placed in 4% paraformaldehyde, pH 7.4, for 60 minutes at room temperature. Retina was washed 6 times for 30 minutes in a modified PBS (mPBS) solution (0.1M, pH 7.4, 0.1% NaN3, 0.5% Triton X-100) at room temperature, blocked for 2 days in mPBS with 3% donkey serum at 4°C and incubated in primary and then secondary antibodies for 5 and 2 days, respectively, in 1% donkey serum in mPBS at 4C. Retinas were washed 4 times for 30 minutes in mPBS before being mounted onto slides, with 4,6-diamidinno-2-phenylindole (DAPI) (0.2µg/mL Sigma-Aldrich) added during the last

wash. We used the following primary antibodies: mouse anti-PKCα (1:100, Santa Cruz Biotechnology, sc-8393), rabbit anti-PKCα (1:100, Santa Cruz Biotechnology, sc-208), mouse anti-CtBP2 (1:400, BD Biosciences, 612044), goat anti-CtBP2 (1:100, Santa Cruz Biotechnology, sc-5966), rabbit anti-mGluR6 (1:1000, a gift from Stephen Massey (Pan and Massey, 2007)), rabbit anti-secretagogin (1:400, Sigma-Aldrich, HPA006641). The following secondary antibodies (1:1000, Life Technologies) were paired with the appropriate primary antibodies: donkey anti-goat 555nm, donkey anti-mouse 488nm or 647nm, and donkey anti-rabbit 488nm or 647nm. PNA 568nm (1:200) was also sometimes added during the secondary incubation period. Retinas were mounted with Vectashield (H-1000; Vector Laboratories).

Imaging and Image Preparation

Lesions were imaged on a Leica SP5 confocal microscope with oil immersion lenses (40x NA 1.25 or 63x NA 1.4). Voxel size was set by 532nm Nyquist values and each optical plane was imaged 3-4 times. ImageJ software (NIH) was used to generate Z-projections and cross sections from Z-stacks.

For most image analysis, measurements were first made in ImageJ by creating regions of interest and then transferring this data to MATLAB (Mathworks) for further processing.

To assess the lesion closure, a mask for the Z-projection of the OPL ribbons was created in MATLAB, and the area lacking ribbons was used to determine an equivalent width of the lesion given that the lesion spanned the entire length of the

image (area of mask = image length * equivalent width of lesion). The same calculation was made for the combined STAs of lesioned retinas to calculate functional closure.

The data on soma location, number of dendrites, dendritic reach, and rod bipolar cell to cone pedicle interactions was first collected on Z-stacks in ImageJ and then analyzed in MATLAB. Definitions for dendritic reach and rod bipolar to cone pedicle interactions follow.

For each dendritic branch, the dendritic reach was measured as a straight-line length from the base of the dendrite at the cell body out to the dendritic terminal farthest from the cell body. PKCα-positive thickened rod bipolar cell dendrites were measured to the extent that they could no longer be distinguished from surrounding dendrites. These measurements are therefore an underestimation of the thickened dendrite's reach. Since all the rod bipolar cells are stained with PKCα, the overlap of their dendritic fields prevented us from measuring the length of individual dendrites in healthy cells. Instead, we measured the dendritic reach of four healthy individually filled rod bipolar cells from mid-inferior rabbit retina (provided by Christopher Whitaker and Stephen Massey, cell-fill photographs not shown). The dendritic reach quantifies the photoreceptor sampling range of a single dendritic branch much the same way the dendritic field area quantifies the photoreceptor sampling range of an entire bipolar cell. To scale the dendritic fields of the filled healthy cells to the $1200\mu m^2$ dendritic field area of the far peripheral retina, a scaling factor, given by

$(1200\mu m^2$ / mean dendritic field area of filled cells$)^{1/2}$, was applied to each dendritic reach. The mean dendritic field area of the filled healthy cells was $636\mu m^2$.

Healthy rod bipolar cell dendrites, scaled to emulate cells in the far peripheral retina (see previous paragraph) did not reach beyond 28µm from the cell body (0 out of 32 dendrites). The frequency of thick restructured rod bipolar cell dendrites reaching beyond 28µm from their cell body to their first synaptic contact was measured to be 6/41 (6 out of 41 cells located inside 4 month old lesion, 28µm or further from the nearest photoreceptor synaptic ribbon). We calculated the probability of these two observations coming from the same underlying distribution using Monte-Carlo simulation. In particular, we simulated 10^{10} results of the binomial experiment where 41 attempts are made with the underlying success probability of 6/41, yielding the number of successes, R. For each R, we simulated a binomial experiment with 32 attempts and underlying success rate of R/41, yielding the number of successes R1. The p-value was calculated as the ratio of the number of times R1 was equal to zero in the 10^{10} attempts. It was found to be: $p = 0.030$ (S.E.M.= 10^{-6}). The uncertainty was estimated by subdividing the 10^{10} attempts into 10^6 groups of 10,000 attempts each, calculating the p-value for each group and then calculating the standard error of the p-value mean.

For each primary dendrite, the dendritic projection was measured as the angle the dendrite left the cell body of secretagogin- and PKCα- positive cells relative to the lesion edge. Some secretagogin-positive cells sent a dendritic stalk vertically toward the outer plexiform layer before branching. If a cell had a vertical stalk, the dendrites

branching off the stalk were considered the primary dendrites and the angles at which they branched from the stalk were measured. If a dendrite between two cells appeared to originate from both somas then it was measured for both cells. A vector sum of each cell's dendrites was created by summing the unit length projection vectors of each measured primary dendrite. The directionality index (DI) for each cell was defined as DI = (exit – enter) / (exit + enter) where exit = number of dendrites projected away from lesion center and enter = number of dendrites projected toward lesion center.

Rod bipolar cell and cone pedicle interactions were classified into three categories while viewing a z-stack with PKCα, CtBP2 and mGluR6 staining in ImageJ. A cone pedicle was marked 'approached' if a rod bipolar cell dendrite terminated within the cone pedicle area (identified by mGluR6 and ribbon morphology) without co-localizing with a rod spherule (identified by a mGluR6 doublet). If a dendrite passed through a cone pedicle to make contact with a rod spherule, the cone was marked 'ignored.' A cone pedicle was 'avoided' if no rod bipolar cell dendrites approached or passed through the cone pedicle. Examples of the three types of interaction between cone pedicle and rod bipolar cell dendrites can be found in Figure 18C. Cone pedicles that could not be categorized due to a very bright rod bipolar cell body obscuring possible approaches were removed from the analysis.

Sprouting events were counted in lesions of various ages using equally sized (50 μm) cross sections from confocal stacks. The number of spouting events counted

was divided by the area of lesion in the 50μm cross section (area of lesion = 50μm * lesion width).

Results

Photopic and scotopic visual sensitivity is restored after photoreceptor ablation

Using a rapidly scanning laser, we selectively coagulated a rectangular patch of photoreceptors in the mid-inferior region of the adult rabbit retina, leaving the inner nuclear layer (INL) intact (Paulus et al., 2011; Lorach et al., 2015). The 1.5mm long line lesion patterns of 100μm, 200μm, and 300μm in width were examined 3 days to 4 months post-procedure. In some cases, acute lesions (under 16 days) were placed next to older lesions (1, 2, and 4 months) in the same retina to provide a reference for structural and functional changes between younger and older lesions.

Examination of the retinas using immunohistochemistry shows that healthy photoreceptors adjacent to the lesion shift into the damaged zone over time. Staining with peanut agglutinin (PNA) to identify cone outer segments and a rabbit anti-protein kinase Cα (PKCα) antibody that outlines rod outer segments shows that the gap in both rod and cone outer segments narrows over time after the injury (Figure 15A). This finding is consistent with previous reports (Busch et al., 1999; Paulus et al., 2008, 2011; Lavinsky et al., 2013; Sher et al., 2013; Strazzeri et al., 2014). Two mechanisms could account for this filling in: photoreceptor outer segments could lean into the lesion, leaving their pedicles and spherules behind, or the entire

photoreceptor could shift into the lesion. To distinguish between these possibilities, we imaged the horseshoe-shaped ribbon structures found at the cone pedicle and rod spherule synapses using an antibody to C-terminal binding protein 2 (CtBP2), which are found in the cells' termini. We find that the width of the gap in ribbon coverage also narrows over time (between 3 and 120 days, Student's t test, $p<0.02$), with most ribbon movement occurring within the first month of ablation (see an example in Figure 15A and the average data based on 151 lesions in 4 rabbits in Figure 15B). After 30 days, there was no additional significant closure of the lesions (Student's t test, $p>0.15$). In 1 of 5 rabbits (31 lesions) we observed no statistically significant change (Student's t test, $p>0.25$) in the ribbon coverage gap (gray lines, Figure 15B). This likely reflects variability observed in the initial damage and healing dynamics between animals. A smaller gap in ribbon coverage remains 4 months after lesioning, even in the areas where the photoreceptor outer segments filled in the initial damage zone (Figure 15A). Therefore, we conclude that the entire photoreceptor shifts into the lesion and their outer segments lean further inward. Both cone and rod ribbon structures (dimmer clustered ribbons and bright horseshoe-shaped ribbons, respectively) are present inside the initial lesion boundaries, indicating that both, cone pedicles and rod spherules can shift into the lesion (Figure 15A).

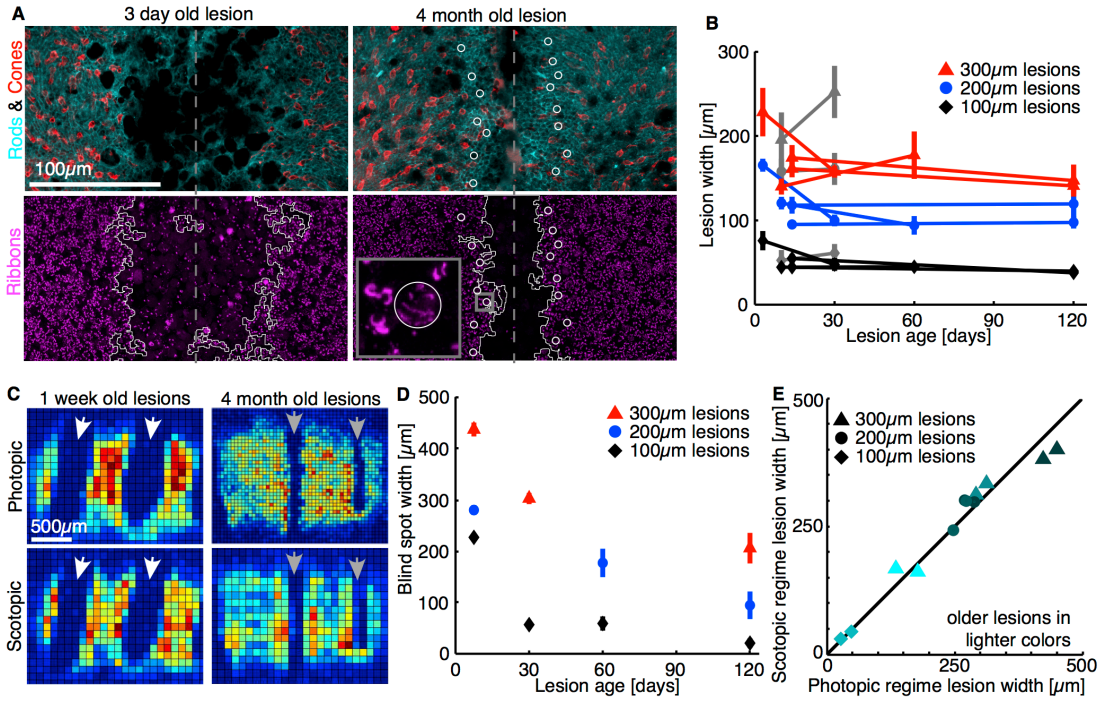

Figure 15. Photoreceptor outer segments and their synapses shift into lesions over time and restore visual sensitivity in the rod and cone pathways.
A, Rod and cone outer segments at the edges of a 3 day and 4 month old 100µm-wide lesion. Lesion center marked by dashed gray line. Ribbons (in the OPL) are visible at the lesion edges. Lesion edges were defined as the solid white outlines, calculated with custom software. Both cone (circled) and rod ribbons are found inside the former lesion edges. B, Lesion width over time, as measured by lack of ribbon coverage (calculated from lesion outlines in (A)). Widths are reported for 100µm, 200µm, and 300µm wide by 1.5mm long laser scanned areas. Lines connect acute (3-16 day) and older (1, 2, or 4 month) lesions placed in the same rabbit. 1 of 5 rabbits did not show lesion closure (grayed out, Student's t test $p > 0.25$). Data is shown as mean ± SEM. C, Examples of visual sensitivity plots, obtained from spike-triggered average sensitivity profiles, in retinas with 300µm lesions. Gaps in visual sensitivity in both the photopic and scotopic regime are much wider in 1 week old lesions (white arrows) than in 4 month old lesions (gray arrows). Pixel size in these maps is defined by the stimulus pixel size. All panels are scaled equally. D, Lesion width as measured by lack of visual sensitivity in the photopic regime over time. Data is shown as mean ± SEM. E, Comparison of visual sensitivity lesion widths in the photopic and scotopic regime (n = 12 lesions).

To determine whether the shifting photoreceptors convey information to the retina, we used a multi-electrode array (Litke et al., 2004) to record responses of the

retinal ganglion cells (RGCs) located within and outside the lesions. Previous work using 200μm diameter spot lesions showed that shifting photoreceptors restored visual sensitivity to the blinded area under photopic conditions, which predominantly measures cone function (Sher et al., 2013). Here we measure rod and cone photoreceptor mediated responses separately. We used binary spatio-temporal white noise stimuli at scotopic and photopic mean luminances (5-13 and 5400 Rh*/rod/sec, respectively) to determine the extent of recovery in both rod and cone pathways. The RGC's spike-triggered average response to a white noise stimulus measures the cell's spatio-temporal receptive field and reveals its spatial sensitivity profile (Chichilnisky, 2001). Combining the receptive fields of all recorded RGCs from a single piece of retina with two 1-week-old line lesions reveals two distinct blind spots under both photopic and scotopic stimulation conditions (Figure 15C). This confirms that laser photocoagulation leads to loss of visual sensitivity in RGC receptive fields. For all three lesion widths (100, 200 and 300 μm), the blind spot narrows over time (between 7 and 120 days, Student's t test, $p<0.03$), as observed across 28 lesions in 7 rabbits (Figure 15C, D). We do not see significant closure in lesions after 30 days (Student's t test, $p>0.09$), which resembles the dynamics of the shifting ribbons. Furthermore, the functional recovery mediated by cone and rod photoreceptors is matched, as shown by a subset of experiments with scotopic and photopic data (n = 12 lesions, 5 rabbits) (Figure 15E).

These results demonstrate that cone and rod photoreceptors shift into the lesioned area, and that their respective pedicles and spherules have functional connections with bipolar cells.

Deafferented rod bipolar cells extend their dendrites toward photoreceptors

To understand how dendritic fields of bipolar cells change in response to local photoreceptor loss, we visualized rod and cone bipolar cells, as well as their pre- and post-synaptic structures, using immunohistochemistry and confocal microscopy on flat mounted retina. The synapses between rod spherules and rod bipolar cells were identified using antibodies against PKCα to stain the rod bipolar cell, metabolic glutamate receptor 6 (mGluR6) to stain the rod bipolar cell glutamate receptor, and CtBP2 to stain synaptic ribbons (Young and Vaney, 1991; Vardi et al., 2000; tom Dieck et al., 2005). In healthy rod bipolar cells, dendritic tips invade the rod spherule to make a synaptic contact (Dacheux and Raviola, 1986). Glutamate receptor mGluR6 is localized to the dendritic tip region within the bipolar cells (Vardi et al., 2000), and appears as a doublet that represents two rod bipolar cells contacting a single rod spherule (Li et al., 2004) (Figure 16A insets).

Deafferented rod bipolar cells lose their dendritic tips and most mGluR6 expression within days of the photoreceptor ablation, without altering the structure of their dendritic trees (Figure 16A). Two weeks post-ablation, the finer dendritic processes start to disappear, and a few bipolar cells restructure their dendrites to have thickened processes directed toward the healthy photoreceptors at the lesion edge (Figure 16A). Over time, deafferented rod bipolar cells significantly restructure their

dendritic trees, such that most dendritic branches are eliminated (Figure 16B). The remaining dendritic branches, which appear thickened, extend toward the edge of the lesion (Figure 16C-E). The thickened dendrites terminate in the ribbon-rich areas of the outer plexiform layer (OPL) and have dendritic tips that co-localize with mGluR6 and rod ribbons (Figure 16D).

On- and Off-cone bipolar cell dendrites, visualized with an antibody against secretagogin (Puthussery et al., 2010) do not undergo the obvious changes we observe in rod bipolar cells. While the dendritic network of the cone bipolar cells is disturbed within the lesion, the mean number of major dendritic branches remains the same inside and outside the lesion at all ages (Student's t test, $p>0.12$, Figure 16F, 2G). Rare examples of a thick process extending toward the healthy photoreceptors are an exception rather than a rule (data not shown).

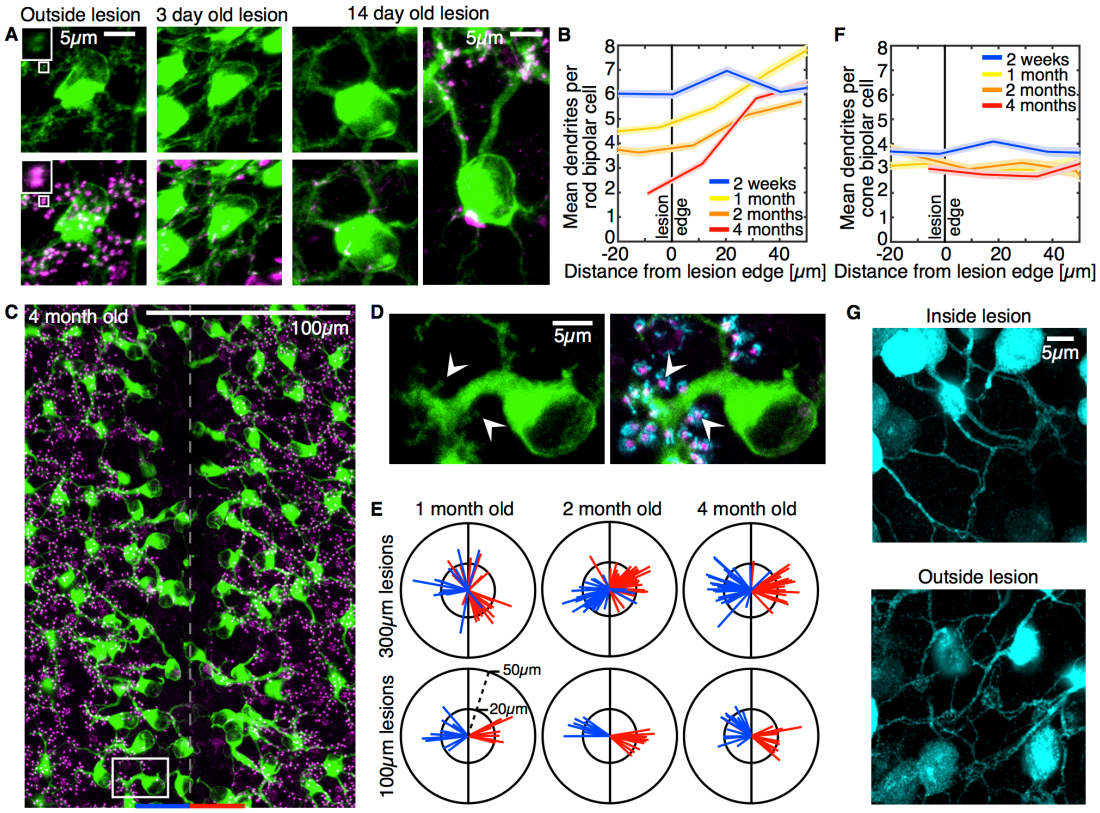

Figure 16. Bipolar cell dendritic trees change in response to photoreceptor loss. A, Dendritic tips of healthy rod bipolar cells (PKCα, green) share a rod spherule with another rod bipolar cell, which is visible as a doublet structure (see insets) of the glutamate receptors (mGluR6, magenta). Rod bipolar cells lose their dendritic tips and glutamate receptors within 3 days of photoreceptor loss. Dendrite simplification and pruning is evident in 14-day-old lesions. Fine processes are lost, leaving only major dendritic branches (see cell on the left). Some cells show signs of asymmetric pruning (see cell on the right); dendrites directed toward a lesion edge (up) are strengthened in comparison to the dendritic branches directed toward the lesion center (down). B, Dendrite pruning in rod bipolar cells of acute and older 200μm lesions in the same rabbit. Data is shown as mean ± SEM. C, Rod bipolar cells and glutamate receptors at the OPL of a 4-month-old 100μm lesion. D, Inset from (C). Dendritic tips are visible at the ends of the thickened rod bipolar cell dendrite (arrowheads). Dendritic tips co-localize with glutamate receptors and ribbons (CtBP2, cyan). E, Projection angle and length of thickened dendrites from rod bipolar cells left (blue) and right (red) of lesion center. Lesion orientation is vertical, shown with black line. F, Dendrites of secretagogin-positive cone bipolar cells in acute and older 200μm lesions in the same rabbit. These lesions are the same lesions as those in (B) and pictured in Figure 3A. G, Cone bipolar cell (secretagogin, cyan) dendrites inside and outside a lesion. Small dendrites are still visible within the lesion, but their network appears abnormal.

To compare the response to deafferentation between the rod bipolar and secretagogin-positive cells we analyzed data from four lesions immunostained at four time points after photocoagulation (Figure 17A). Both rod bipolar cells and secretagogin-positive cone bipolar cells were labeled in each of the four retinal pieces, providing for the direct comparison. We measured the projection angle of all primary dendrites extending from each cell inside and outside of each of these lesions. The dendritic projections of each cell's dendrites were then added vectorially to obtain a single vector representing the dendritic projection of each cell (Figure 17B). In this vector sum, each dendrite was weighted equally, regardless of its total length or thickness. Dendritic projections of rod bipolar cells show a bias toward the lesion edge (Figure 17C), which correlates with the preferred direction of the thickened dendrites (Figure 16E). However, the distribution of the secretagogin-positive cells' dendritic projections did not show such an obvious bias (Figure 17C). To quantify the difference between the two cell types, we calculated the directionality index (DI, see Methods) of each cell. Cells with no directional preference in their primary dendrites had a DI value of zero. A DI value of +1 or -1 meant that a cell directed all of its dendrites away from or toward the lesion center, respectively. The DI index was calculated for each of the lesions in Figure 17A, and separately for rod bipolar and secretagogin-positive cone bipolar cells located inside and outside the lesion. Secretagogin-positive cells inside the lesion have the same DI as those outside the lesion, confirming that their dendrites do not restructure in a preferred direction

from the cell body (Kolmogorov-Smirnov test $p>0.67$, Figure 17D). Rod bipolar cell dendrites show significant bias to project out of the lesion at 2 and 4 months ($p<0.01$, Figure 17D). Deafferented rod bipolar cells project their dendrites, including the thickened ones, toward the lesion edge, while deafferented secretagogin-positive cells do not form thickened dendrites, nor do they direct their dendrites toward the lesion edge.

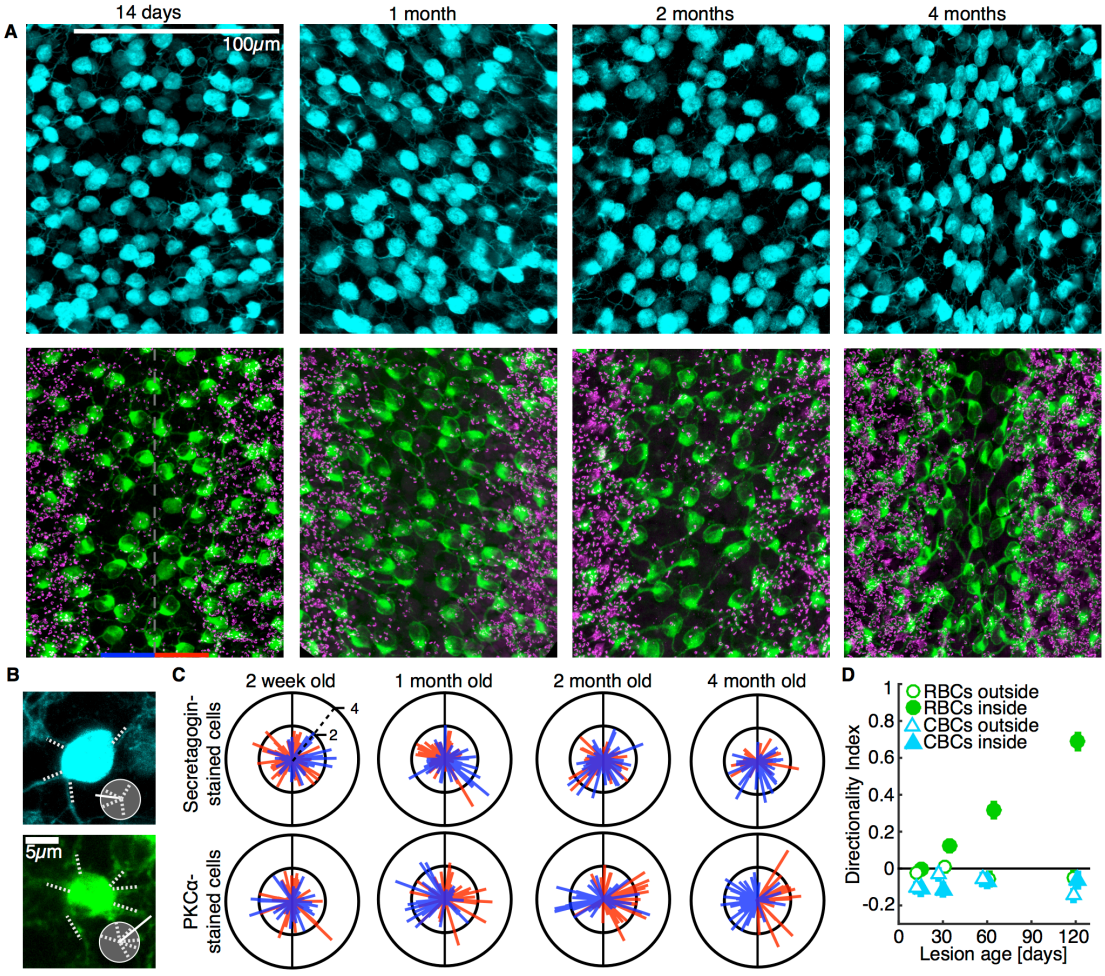

Figure 17. Rod and cone bipolar cells within the same lesion do not restructure their dendrites in the same manner.

A, Cone bipolar cells (secretagogin, cyan) within 200μm lesions at 14 days, 1 month, 2 months and 4 months. Rod bipolar cells (PKCα, green) in the same field of view as the cone bipolar cell images. Ribbons (CtBP2, magenta) in the rod bipolar images show lesion edges. B, Example vector sum calculations for a cone (secretagogin, cyan) and rod (PKCα, green) bipolar cell. Measured dendrite projection angles (dashed white lines slightly offset from dendrites) are placed in a unit circle (gray circle) and summed to create a dendritic projection vector (solid white line) for each cell. C, Dendritic projection vector sum analysis of the four lesions pictured in (A). Dendritic projection vectors representing all dendrites from cone and rod bipolar cells left (blue) and right (red) of lesion center. Lesion orientation is vertical, shown with black line. D, The directionality index of cone and rod bipolar cell dendrites inside or outside of a lesion. Rod bipolar cells (RBCs) inside 2 and 4 month old lesions bias their dendrites to exit the lesion (Kolmogorov-Smirnov test, $p<0.01$). Secretagogin-stained cone bipolar cells (CBCs) do not bias their dendrites to exit the lesion ($p>0.67$).

Rod bipolar cells synapse with rods outside of their original dendritic territory

Two distinct mechanisms can result in the rod bipolar cells' thickened dendritic process extending toward healthy photoreceptors. First, the laser ablation could remove all photoreceptor inputs to the bipolar cell except one, and this could lead to the removal of unoccupied synapses, pruning of the deafferented portion of the dendritic tree, and strengthening of the remaining functional dendrite. Alternatively, deafferented rod bipolar cells could restructure their dendrites to project into territory that has functional photoreceptors, where they can form new synapses.

In order to test if the rod bipolar cells extend their dendrites to form new synapses with healthy photoreceptors, we compared the dendritic reach of healthy rod bipolar cells to the reach of thickened dendrites found within lesioned retina. Due to the overlap of dendritic fields from PKCα-positive cells, we could not discern the dendritic field of an individual healthy cell. Instead, we measured the dendritic reach

of four healthy individually filled rod bipolar cells from mid-inferior rabbit retina (provided by Christopher Whitaker and Stephen Massey, cell-fill photographs not shown). For the filled cells, we measured the straight-line distance between each dendrite's exit from the soma and its distal termination at the edge of the dendritic field. These distances (32 dendrites from 4 cells) provided the distribution of the dendritic reach for the healthy rod bipolar cells. (See Methods for details on the comparisons between PKCα-positive cells and filled cells.)

The dendritic reach of the thickened dendritic processes of the deafferented rod bipolar cells is significantly (Kolmogorov-Smirnov test $p<1E\text{-}8$) longer than that of healthy rod bipolar cells. Since the dendritic field size of rod bipolar cells changes with eccentricity (Young and Vaney, 1991), we wanted to ensure that the observed difference was not caused by comparing cells from different retinal locations. The significant ($p<0.01$) difference between the reach of the restructured dendritic processes and that of the healthy dendrites remained even after we scaled up the dendritic fields of the filled cells to reach the maximum reported rod bipolar cell dendritic field area of $1200\mu m^2$ (Young and Vaney, 1991) (Figure 18A, see Methods for details of the scaling procedure). This area corresponds to 10mm eccentricity in the superior retina, which contains cells with dendritic fields larger than anywhere in the inferior retina, where lesions were actually placed.

The shift of the distribution toward longer dendritic reach is not simply a result of shorter dendrites being pruned away. We observe the increase in dendritic reach ($p<0.001$) even in narrow lesions, where 98% of rod bipolar cells (49 of 50

cells) extend a thickened dendrite. Such a result cannot be achieved through a passive pruning process, unless all the original rod bipolar cell dendritic fields coincidentally had a longer reach in the direction perpendicular to the future lesion.

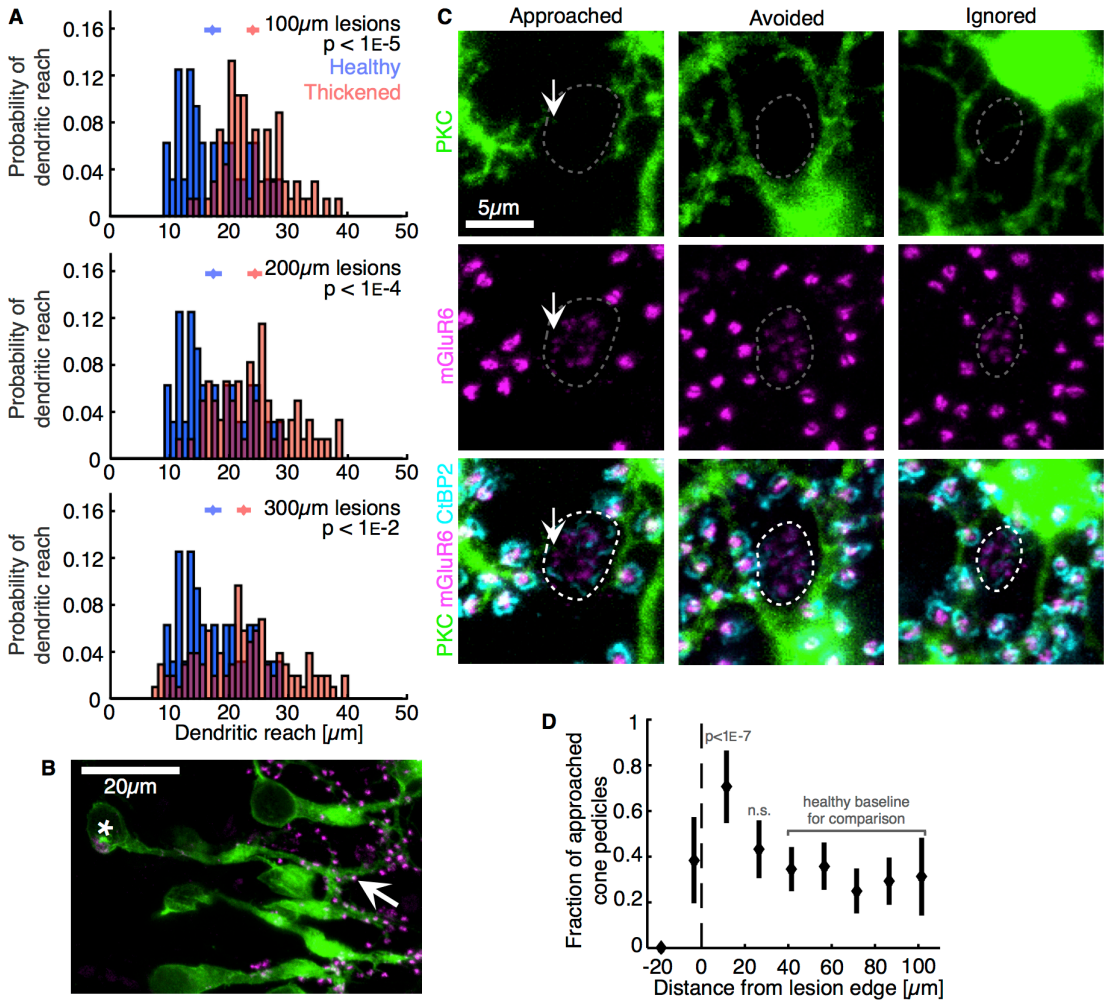

Figure 18. Rod bipolar cells actively search for new synaptic partners.
A, The dendritic reach of healthy rod bipolar cell dendrites (blue) and thickened dendrites (red) in 100µm, 200µm and 300µm lesions. Mean ± SEM are shown above the two populations and p-values from the Kolmogorov-Smirnov test are printed for each lesion size. B, Example rod bipolar cell (*) in a lesion with a 45µm dendritic reach making synaptic contact outside the lesion, shown by an mGluR6 doublet located distally on the dendrite (arrow). C, Examples of cone pedicles (outlined by dashed shape) being approached, avoided, or ignored by a rod bipolar cell dendrite. Typically, rod bipolar cell dendritic tips (PKCα, green) terminate at rod spherules

(mGluR6 doublets, bright magenta outside dashed shape). Occasionally, a rod bipolar cell dendritic tip terminates within a cone pedicle (arrow). D, Fraction of cone pedicles that are approached by a rod bipolar cell dendrite. Fractions are given as mean ± SEM and p-values are calculated using unpooled binomial statistics.

So far, we have not differentiated rod bipolar cells that have been completely deafferented, restructured their dendrites and formed new connections from rod bipolar cells that have been partially deafferented and have extended their dendrites further into photoreceptor-rich areas to form new connections. We performed the following analysis to test if some remaining synapses are necessary for the formation of new synapses. If only partially deafferented rod bipolar cells are capable of synaptogenesis then the original dendritic reach of a restructured rod bipolar cell is determined by the dendritic reach distribution of healthy cells. Under this hypothesis, we estimated the minimum original dendritic reach of the restructured cells to be the distance from the cell body to the first synapse located on the restructured thick dendrite. In healthy rod bipolar cells, zero out of 32 dendrites reach beyond 28µm from the cell body. At the same time, in a 4 month old 300µm wide lesion, 6 out of the 41 rod bipolar cells located 28µm or further from the nearest photoreceptor synaptic ribbon extended a dendrite that could be traced to a synaptic contact. The two results do not come from the same distribution ($p=0.03$ using binomial statistics: see Methods) indicating that some of the rod bipolar cells with long restructured dendrites were completely deafferented and then formed new synapses with healthy photoreceptors.

These findings, combined with synaptic contacts found at the extremities of all the lengthened dendrites we could trace (Figure 18B), show that rod bipolar cells in the adult rabbit retina are capable of sending dendritic projections well beyond their original dendritic field territory to synapse with rod photoreceptors.

Next, we asked if the dendrites of deafferented rod bipolar cells selectively target rod photoreceptors or if they approach cone pedicles as well. Cone pedicles can be distinguished from rod spherule synaptic contacts by differences in the mGluR6 expression pattern and ribbon synapse structure (Li et al., 2004); rod spherules are marked by bright mGluR6 doublets and bright horseshoe-shaped ribbons, while cone pedicles appear as small clusters of mGluR6 puncta and dimmer clustered ribbons (cone pedicles outlined by dashed shape, Figure 18C). To determine whether rod bipolar cells selectively target rod photoreceptors after deafferentation, we measured the frequency of a cone pedicle being approached, rather than bypassed by a rod bipolar cell dendrite as a function of cone location relative to the lesion edge. Cone pedicles were bypassed by rod bipolar dendrites in one of two possible ways: avoided or ignored. (See methods for details on approached, avoided and ignored labels and see Figure 18C for examples.) We find that cone pedicles just outside the lesion edge are significantly more likely to be approached than bypassed by a rod bipolar cell dendrite compared to cone pedicles in the intact healthy areas ($p<1E\text{-}7$, using unpooled binomial statistics based on 298 cones) (Figure 18D). We do not have the necessary resolution to determine whether the rod bipolar cell dendrites that terminate within a cone pedicle make synaptic contact with the cone. Thus, this data suggests

that either the adult deafferented rod bipolar cell dendrites are less selective in choosing synaptic partners, or that they explore potential afferents before making contact. Interestingly, of the 112 approached cone pedicles, only 2 were approached by more than one rod bipolar cell dendrite.

New synaptic partners for deafferented rod bipolar cells reverse sprouting

Photoreceptor damage or disease often leads to dramatic changes in retinal structure. In response to photoreceptor malfunction, bipolar cells send dendritic sprouts into the outer nuclear layer (ONL) that can sometimes result in ectopic synapses (Haverkamp et al., 2006; Sullivan et al., 2007). In our injury model, rod bipolar cells also exhibit initial sprouting and ectopic synapses in the ONL (arrowheads, Figure 19A); however, they decrease over time (Figures 5A-B). This observation indicates that, if provided with healthy presynaptic partners, rod bipolar cells will prune "incorrect" sprouts in the ONL in favor of making contacts with rods in the OPL.

Axon terminal atrophy is also commonly reported in animal models of retinal degeneration (Strettoi and Pignatelli, 2000; Strettoi et al., 2003; Barhoum et al., 2008). Deafferented rod bipolar cells with restructured dendrites maintain their axons and terminals in the ON inner plexiform layer (Figure 19A). Axon terminals are not disfigured and retain coverage of the inner plexiform layer (Figure 19C).

We find that rod bipolar cell somas within the lesion area can move vertically toward the ONL or deeper into the INL (Figure 19A). Cell soma movement out of their original layer is known to occur during advanced stages of retinal degeneration

(Jones and Marc, 2005). Here we observed cellular displacement at a much smaller scale: less than 20% of cells within the 4 month old 300µm lesion pictured in Figure 19A appear vertically displaced (n = 29 of 176 cells). We observed similar displacements in 4 month old lesions of all initial widths. The lateral shift of the rod bipolar cell bodies, indicated by their axons angled toward the lesion center (Figure 19A) and manifested by higher density of bipolar cell soma within 4 month old lesions (Figure 17A), is probably caused by wound contraction.

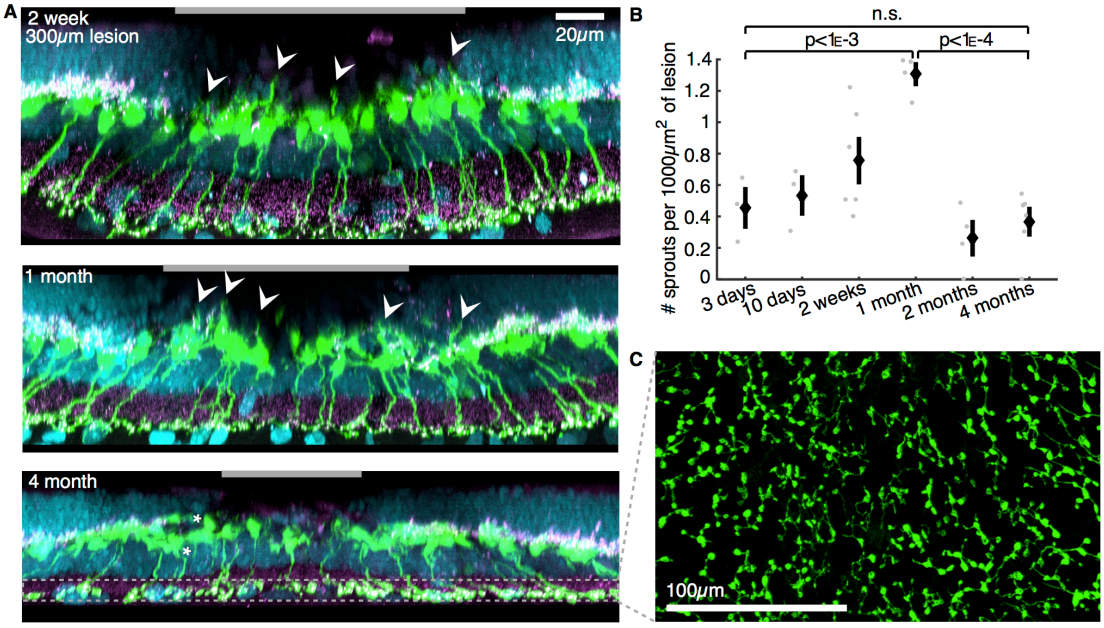

Figure 19. Sprouting, but not cell body movement, is reversed in recovering lesions. A, Cross sections of confocal Z-stacks of 2 week, 1 month, and 4 month old lesions. Rod bipolar cells (PKCα) are shown in green, ribbons (CtBP2) in magenta, and DAPI is in cyan. Rod bipolar cells have axons and axon terminals at all lesion ages. Dendritic sprouts (arrows) are common in 2 week and 1-month-old lesions, but not present at 4 months. In the 4-month-old lesion, asterisks (*) mark two example cells that have moved vertically (up and down) out of their normal layer. Horizontal gray bars show width of ONL missing (DAPI stained) photoreceptor cell bodies. Variation in retinal thickness between these cross sections results from variable squashing of the tissue during electrophysiological recording. B, The frequency of sprouting rod bipolar cells in 300µm lesions (gray dots) over time. Mean ± SEM are shown with p-values from the Student's t-test. C, Axon terminals of rod bipolar cells within a 4

month old lesion, viewed as a maximal Z-projection, as indicated by the dashed box in (A).

Discussion

This study demonstrates synaptogenesis in the adult mammalian retina, which recovers the flow of visual information through both scotopic and photopic circuitry. After a patch of photoreceptors is selectively destroyed by laser photocoagulation, healthy photoreceptors surrounding the lesion shift laterally into the damage zone, together with their synaptic terminals. Visual sensitivity is restored in the previously blinded areas at both scotopic and photopic light levels. Rod bipolar cells drastically prune and restructure their dendritic tree and synapse with healthy rod photoreceptors. In contrast, cone bipolar cells maintain their primary dendrites and do not bias their dendritic fields toward remaining photoreceptors. Sprouting of rod bipolar cell dendrites, an early sign of retinal degeneration, is reversed in favor of new rod afferents. These observations demonstrate an innate ability of the adult mammalian retina to repair damage caused by injury or disease and is encouraging for the photoreceptor reintroduction approach to restoration of sight.

Adult rod bipolar cells are capable of normal synaptogenesis

Examination of the functional and structural dynamics of rod and cone photoreceptors, their synapses, and their post-synaptic partners after ablation of photoreceptors reveals the following processes: initial loss of the photoreceptor outer segments, cell bodies, and ribbon synapses matched on the post-synaptic side with a

disappearance of mGluR6 in the dendrites of rod bipolar cells, which complements findings from a report on mouse cone bipolar cells (Dunn, 2015). By 4 months, both rods and cones from adjacent areas have shifted into the lesion along with their synaptic terminals, creating new synaptic possibilities inside the lesioned area. Rod bipolar cell dendrites extend out of the lesioned space, supporting the hypothesis that shifting photoreceptors are making new contacts rather than simply dragging old contacts with them (Figure 16E) (Sher et al., 2013). Synapses near the lesion appear structurally normal, and are indistinguishable from synapses in the intact areas. Restoration of visual sensitivity in the former blind spot over time indicates that these shifting synapses are functional, both at the cone pedicle and rod spherule.

A new synaptic contact between a rod and rod bipolar cell is not limited by proximity; rod bipolar cells project dendrites over long distances to form new connections. This projection is directed to the nearest edge of the lesion, suggesting that some signal from the healthy photoreceptors is guiding the dendrites. These dendrites approach not only rod spherules but also cone terminals. Some of these approaches may result in a cone to rod bipolar cell synapse, which is known to occur in both the healthy and diseased retina (Dacheux and Raviola, 1986; Peng et al., 2000; Strettoi et al., 2004). However, in diseased retina, cone to rod bipolar cell synapses were shown to occur more frequently than in healthy retina (Peng et al., 2000). We also observed an increase in such approach events at the lesion edge, indicating that though deafferented adult rod bipolar cells form new synapses with rods, they may also synapse with cone photoreceptors.

Rod and cone pathways differ in their plasticity

We observed dramatic dendritic rearrangements of the deafferented rod bipolar cells, but secretagogin-positive cone bipolar cell dendrites do not restructure in the same manner. Deafferented secretagogin-positive cells maintain the number of their primary dendrites and do not project their processes out of the lesion. We did note that secretagogin-positive cone bipolar cell dendrites had, on average, a small negative directionality index, indicating the dendritic trees are slightly biased toward the center of the lesions (Figure 17D). This bias is already present at 14 days in both deafferented cells within and unaffected cells outside the lesion, and hence is likely cause by wound contraction after photocoagulation, that pulls the tissue toward the lesion center. This pull is evident in the leaning of the rod bipolar cell axons toward the lesion center (Figure 19A).

Unlike for the rod bipolar cells, imaging of the secretagogin-positive bipolar cells did not allow us to ascertain if the deafferented cone bipolar cells form new synapses with the shifted photoreceptors. Both photopic and scotopic vision is partially restored after photoreceptor ablation, indicating that the shifting photoreceptors have functional synapses. Previous work revealed that cone bipolar cells, as a population, regain light sensitivity after deafferentation, thus indicating some synaptogenesis (Sher et al., 2013). Secretagogin-positive bipolar cells are only a subset of that population. Studies of additional cone bipolar cell types are needed to better understand the response to deafferentation within the cone pathway.

Variations in dendritic restructuring between the rod and secretagogin-positive cone bipolar cells demonstrates that there are different cellular level mechanisms behind the response to deafferentation and restoration of function in rod and cone circuits. The difference in the mechanisms of adult rod and cone bipolar cell rewiring to their new pre-synaptic partners is not necessarily a surprise. It has been reported that three cone bipolar cell types within the developing mouse retina find and establish cone contacts using unique strategies (Dunn and Wong, 2012). It has also been shown that the underlying molecular mechanisms required for proper connectivity between photoreceptors and bipolar cells during development differ between the rod and cone pathways (Cao et al., 2015). Identifying the molecular mechanisms behind the dendritic expansion and synaptogenesis in the adult retina requires further work.

Sprouting may be reversible if photoreceptors become available

Sprouting of dendrites into inappropriate locations is an early response to retinal degeneration triggered by photoreceptor cell death (Marc et al., 2003). The human retina has been shown to exhibit sprouting of rod bipolar cell dendrites and ectopic synapses in the outer nuclear layer in response to local loss of photoreceptors during age-related macular degeneration (Sullivan et al., 2007). Similarly, the rod bipolar cell dendrites in the adult rabbit retina sprout into the outer nuclear layer after loss of photoreceptors, and occasionally make ectopic synapses. We find that dendrites sprouting into the outer nuclear layer are abandoned in favor of new

contacts in the outer plexiform layer. New pre-synaptic partners may eliminate this particular unwanted plastic response.

Implications for vision restoration in humans

The results of this study provide new insight into the capability of the adult mammalian retina to form synapses with new afferents, and show the differences between bipolar cell types regarding this capability. However, it is important to recognize that the restructuring we describe here may differ across species. For example, in the primate (including human) retina, each midget bipolar cell contacts a single cone photoreceptor in the fovea region, providing high visual acuity. Therefore, the midget bipolar cells constitute the vast majority of bipolar cells in the central primate retina. Given the differences we observe between the rod and secretagogin-positive cone bipolar cell dendritic restructuring in the rabbit retina, it is hard to predict how well primate midget bipolar cells will connect to newly introduced photoreceptors. Future studies will need to address this important question.

Since in our experiments the surrounding healthy photoreceptors were already connected to the retina, it remains unknown whether these preexisting connections with post-synaptic partners facilitated or hindered synaptogenesis with the deafferented rod bipolar cells. This is one of many potential factors that might affect the success of photoreceptor reintroduction into degenerate retina.

Another factor that is likely to affect the success of photoreceptor reintroduction is its timing relative to the degeneration progression. The chances of

success in restoration of proper retinal wiring are likely to diminish after the complete loss of photoreceptors due to the movement of ganglion cells and the formation of aberrant connections occurring at this late stage (Jones and Marc, 2005; Jones et al., 2012). Our findings suggest that partially and completely deafferented rod bipolar cells, which are both likely present prior to the complete loss of photoreceptors, will be able to recruit new pre-synaptic partners in the event of successful photoreceptor reintroduction earlier in disease progression.

Bipolar cells, not photoreceptors, find new synaptic partners

The success of photoreceptor reintroduction therapies critically depends on the ability of the deafferented bipolar cells to establish synapses with the new photoreceptors. Our results indicate that the adult mammalian retina is capable of establishing new functional connections between bipolar cells and photoreceptors. We show that in the rod pathway, it is the rod bipolar cells rather than photoreceptors that prompt synaptogenesis. Dramatic changes in the dendrites of the rod bipolar cells contrasts with the lack of restructuring in the cone bipolar cells. These differences show that various mechanisms for synaptogenesis operate separately within different bipolar cell types after deafferentation. Deciphering these mechanisms will advance the effort to restore vision in degenerating retinas.

Selective S-cone to S-cone bipolar cell wiring exists after photoreceptor loss

The ground squirrel retina is a cone dominant retina and is known to have selective S-cone to S-cone bipolar wiring which is important for blue/yellow color vision. In the following sections I apply the same principles to the ground squirrel retina as I did with the rabbit retina. Photocoagulation lesions were titrated to the ground squirrel retina. I use an antibody that stains the S-cone bipolar cell to investigate its plasticity after deafferentation.

Introduction

We recently showed that rod bipolar cells in the rabbit retina can rewire with nearby surviving photoreceptors after their original afferents were ablated. The dramatic restructuring we observed in the rod bipolar cell dendritic trees was not present in a subset of cone bipolar cells, suggesting that different bipolar cell types have access to different plasticity mechanisms in the adult retina. It remains unknown if deafferented bipolar cells responsible for encoding color, which requires wiring specificity to cone types, are capable of rewiring correctly in the adult retina.

Here, we take advantage of the ground squirrel retina, which is known to have a one-to-one S-cone to S-cone bipolar cell connection, to test if synaptic wiring required for color encoding bipolar cells is possible in the adult retina. We use laser photocoagulation to selectively ablate a small area of photoreceptors, leaving S-cone bipolar cells within the ablation zone completely deafferented but otherwise unharmed. We find that S-cone bipolar cells, which normally have a single vertical

dendritic stalk ascending to a single s-cone, branch profusely in response to deafferentation. The dendritic branches are maintained within the OPL but are not oriented in a preferred direction with respect to the remaining nearby photoreceptors. Some deafferented S-cone bipolar cells make contact with new S-cones. S-cone bipolar cells that find new pre-synaptic S-cones do not reduce their dendritic trees back to a single stalk.

Methods

Selective Photocoagulation

Adult thirteen-lined ground squirrels were used in accordance with the Association for Research in Vision and Ophthalmology Statement Regarding the Use of Animals in Ophthalmic and Vision Research. Squirrels, of either sex, were first anesthetized briefly with isoflurane and then injected intramuscularly with a solution of ketamine hydrochloride xylazine diluted with sterile water. Once the squirrels were anesthetized, typically within 15 minutes post-injection, a single drop of both 1% tropicamide and 2.5% phenylephrine hydrochloride was applied to each eye to dilate the pupil. Lesions were applied to both the superior and inferior retina with a scanning laser (PASCAL, 532nm) using a custom scanning software. A laser beam of 100μm in diameter was scanned once over 1.0mm length of the retina at 1.0m/s scanning velocity and power of 2.0W. Laser settings were titrated in preliminary experiments that checked for photoreceptor destruction with immunohistochemistry.

Line lesions showed an immediate whitening of the fundus when placed, in vivo, in squirrel retinas. Lesions of 200µm in width were created by overlapping 100µm-wide scans, such that the overlap was equal to half the beam diameter.

Immunohistochemistry

Pieces of retinal tissue were separated from the choroid and sclera and placed in 4% paraformaldehyde, pH 7.4, for 12 minutes at room temperature. If a piece of retina had been used for an electrophysiology recording then the choroid was left attached. Retina was washed 6 times for 30 minutes in a modified PBS (mPBS) solution (0.1M, pH 7.4, 0.1% NaN3, 0.5% Triton X-100) at room temperature, blocked for 2 days in mPBS with 3% donkey serum at 4°C and incubated in primary and then secondary antibodies for 5 and 2 days, respectively, in 1% donkey serum in mPBS at 4C. Retinas were washed 4 times for 30 minutes in mPBS before being mounted onto slides, with 4,6-diamidinno-2-phenylindole (DAPI) (0.2µg/mL Sigma-Aldrich) added during the last wash. We used the following primary antibodies: rabbit anti-HCN4 (1:400, Alomone Labs, APC-052), goat anti-S-opsin (1:100, Santa Cruz Biotechnology, sc-14363), goat anti-iGluR5 (1:50, Santa Cruz Biotechnology, sc-7616), mouse anti-CtBP2 (1:400, BD Biosciences, 612044), goat anti-CtBP2 (1:100, Santa Cruz Biotechnology, sc-5966), rabbit anti-secretagogin (1:400, Sigma-Aldrich, HPA006641), mouse anti-CD15 (1:100, BD Biosciences, 559045). Occasionally, to improve our ability to locate S-cone pedicles, goat anti-S-opsin and goat anti-iGluR5 were paired together in the same primary incubation period. The following secondary antibodies (1:1000, Life Technologies) were paired with the

appropriate primary antibodies: donkey anti-goat 555nm or 647nm, donkey anti-mouse 488nm, 555nm or 647nm, and donkey anti-rabbit 488nm, 555nm or 647nm. Retinas were mounted with Vectashield (H-1000; Vector Laboratories) on a glass slide, photoreceptor-side down, with small pieces of molding clay between the slide and the coverslip. The molding clay was carefully depressed until the coverslip rested against the retina.

Image Acquisition and Image Analysis

Lesions were imaged on a Leica SP5 confocal microscope with an oil immersion lens (63x NA 1.4). Voxel size was set by 532nm Nyquist values and each optical plane was imaged 3-4 times. Fiji software (NIH, (Schindelin et al., 2012)) was used to generate Z-projections and cross sections from Z-stacks. Fiji plugins Pairwise Stitching and Grid/Collection Stitching were both used to stitch tiled images (Preibisch et al., 2009).

HCN4-stained bipolar cell dendritic trees were traced using the Fiji plugin Simple Neurite Tracer (Longair et al., 2011). Completed traces were imported to custom MATLAB (Mathworks) scripts. S-cone pedicle locations, identified by a lack of iGluR5 staining (Li and DeVries, 2004) and lesion edge traces, were marked as regions of interest (ROIs) in Fiji and then imported to MATLAB. The OPL was created into a ROI by creating a binary image of an iGluR5 or CtBP2 stain and dilating and then closing the image in 3D (Legland et al., 2016). The OPL was defined by the binary image after an additional dilation step that used a horizontal line to close the ablation zone. In MATLAB, dendritic trees of HCN4-stained bipolar cells

were defined as the traces that overlapped with the OPL. In some cases we distinguish edge HCN4-stained bipolar cells from other cells. Cells were defined as edge cells if they had dendritic trees that crossed the ablation zone edge. The distance from the ablation zone edge to a cell was defined as the smallest distance between the ablation zone edge and the first point the dendritic tree enters the OPL. Dendritic tree fields were defined as convex polygons that outlined the dendritic tree of traced cells. Dendritic field area was the area of this polygon. To calculate dendritic projection vectors, the angle of each dendritic branch with respect to the lesion (ignoring Z) was calculated, and summed, weighted by dendritic branch length with the other dendritic branches.

Results

Localized photoreceptor ablation completely deafferents S-cone bipolar cells.

We used immunohistochemistry to identify S-cones and S-cone bipolar cells in the ground squirrel retina after using laser photocoagulation to selectively ablate a small patch of photoreceptors. In the ground squirrel retina, S-cone bipolar cells can be identified by HNC4 staining (Puller et al., 2011). S-cone pedicles are distinguishable from M-cone pedicles by looking for ribbon synapses lacking iGluR5 (Figure 20C) (Li and DeVries, 2004). An antibody against S-opsin, which brightly stained the outer segments of S-cones, also helped locate S-cone pedicles.

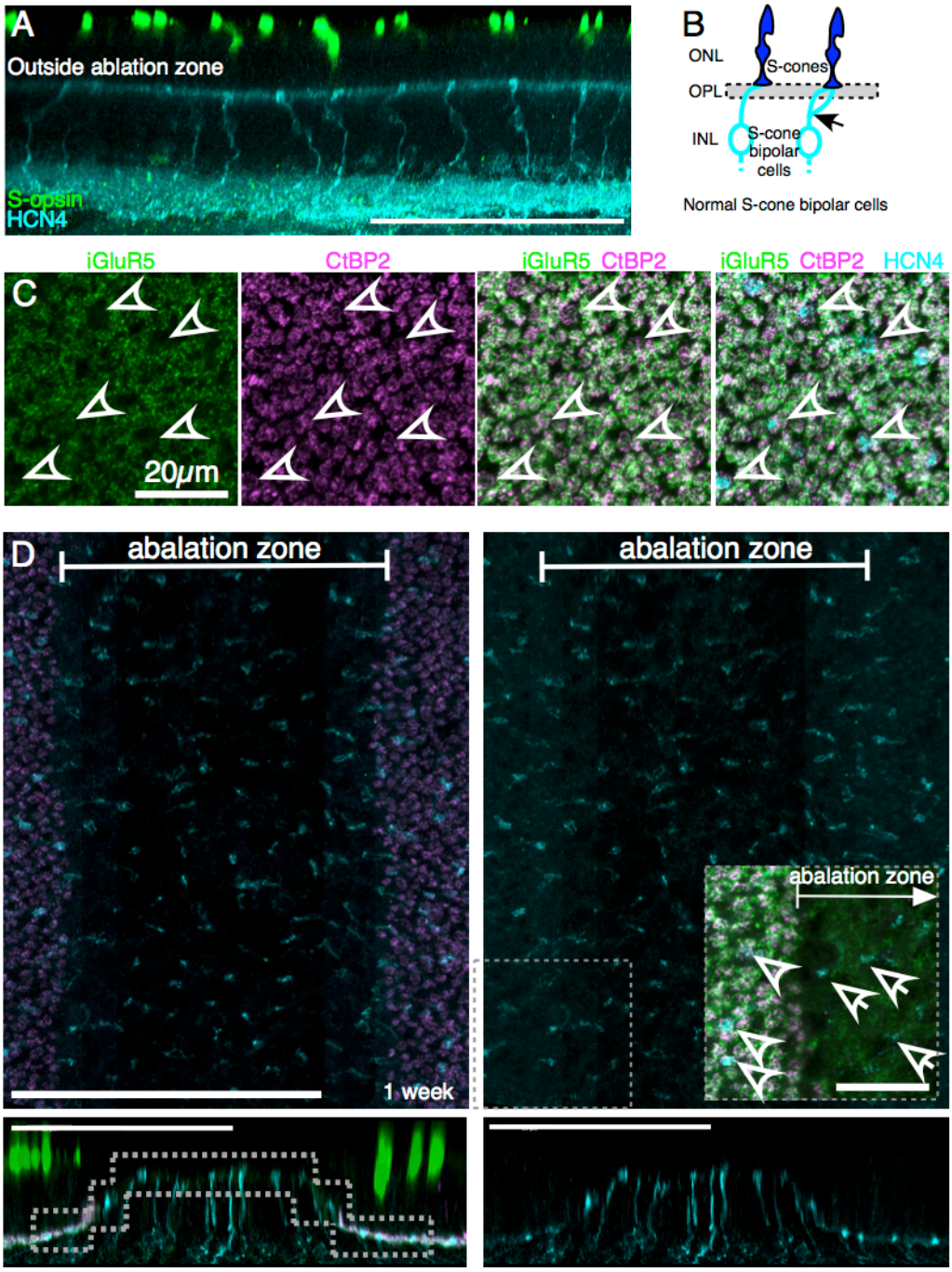

Figure 20. S-cone bipolar cells are completed deafferented by local photoreceptor ablation.

A. Cross section of HCN4-stained S-cone bipolar cells (cyan) in the healthy retina typically extend a single dendritic stalk vertically to contact a single S-cone (outer segments in green). Scale bar 100μm. B. A schematic of S-cone bipolar cells in the healthy retina, aligned with cross section of retina in A. A single dendritic stalk

makes contact with a single S-cone (left). Occasionally, the dendritic stalk branches below the OPL (arrow at right) and returns to the same S-cone. C. In a retinal maximal Z-projection, S-cone pedicles are distinguishable from M-cone pedicles by a lack of iGluR5 (arrowheads point to examples) at cone pedicles (identified by CtBP2 –stained ribbons, magenta). The dendritic tips of HCN4-stained S-cone bipolar cells are visible at S-cone pedicles. D. In a maximal Z-projection (see dashed shape in cross section for regions selected), dendritic tips of S-cone bipolar cells are visible 1-week-post ablation. The ablation zone is identified by a lack of ribbons (CtPB2, magenta). S-cone dendritic stalks extend vertically towards the OPL (cross sections, HCN4, cyan). Scale bars 100µm. Inset: Dendritic tips are visible inside the ablation zone (arrows) where ribbons (magenta) are missing and iGluR5 (green) staining is reduced. Immediately outside the ablation zone dendritic tips make contact with S-cones (arrowheads). Scale bar in inset 20µm.

S-cone bipolar cells in the ground squirrel retina are normally afferent to a single S-cone (Li and DeVries, 2006; Puller et al., 2011). S-cone bipolar cell dendritic trees consist of, typically, a single stalk (Figure 20A, B). Occasionally in healthy retina, a stalk branches and either returns to the primary stalk or, more rarely, contacts another S-cone (Puller et al., 2011). Dendritic branches in the normal retina originate between the cell body and the OPL and ascend towards the OPL (Figure 20B).

Since the S-cone bipolar cell dendritic field is small (consisting of a single cone), local photoreceptor ablation completely deafferents these cells (Figure 20D). Photoreceptor ribbons are absent from the lesion and iGluR5 is reduced within the acute lesion (Figure 20D). The dendritic tips of S-cone bipolar cells remain near the OPL and appear undisturbed. We sometimes observe a hump in the tissue at the ablation zone. We attribute this warping to mechanical strains on the tissue due to photoreceptor loss and wound contraction because the hump is visible in both acute and older lesions (Beier et al., 2017). For Z-projection image clarity we take Z-

projections from smaller sections of the OPL and stitch the sections back together (Figure 20D).

Deafferented S-cone bipolar cells increase their dendritic field

In response to deafferentation, S-cone bipolar cells branch profusely, which increases their dendritic territory (Figure 21). Dendritic branches become apparent in 2 week old lesions and are still visible in 4 month old lesions (Figure 21A, B).

New dendritic branches do not have the same characteristics of dendritic branches occasionally found on healthy bipolar cells. Branches on deafferented cells travel perpendicularly to the primary vertical stalk within the outer plexiform layer (Figure 21D, E). The new dendritic branches begin near the OPL. On healthy cells, however, the occasional branches we observe begin closer to the cell soma (Figure 20B). The number of dendritic branches that begin near the S-cone bipolar cell somas is relatively consistent in the lesioned and healthy tissue (Figure 21F). Furthermore, the dendritic branches on a single deafferented cell appear to emanate in different directions, rarely terminating in the same place, which contributes to a significant increase in the dendritic field of cells in older lesions (Figure 21G, KS test $p <= 0.02$ after 1 month).

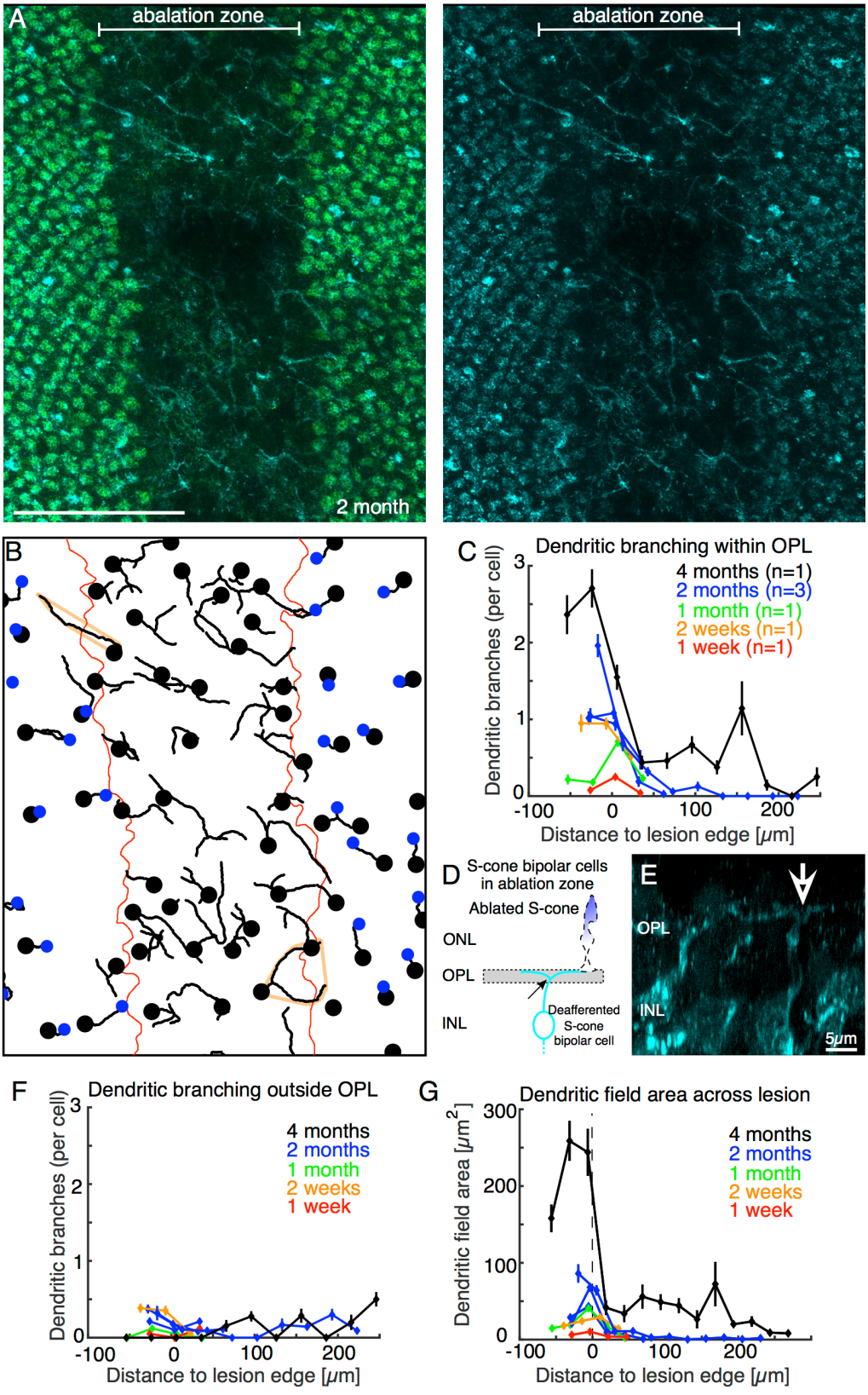
A
abalation zone
2 month
abalation zone
B
C
Dendritic branching within OPL
4 months (n=1)
2 months (n=3)
1 month (n=1)
2 weeks (n=1)
1 week (n=1)
Dendritic branches (per cell)
Distance to lesion edge [μm]
D
S-cone bipolar cells in ablation zone
Ablated S-cone
ONL
OPL
INL
Deafferented S-cone bipolar cell
E
OPL
INL
5μm
F
Dendritic branching outside OPL
4 months
2 months
1 month
2 weeks
1 week
Dendritic branches (per cell)
Distance to lesion edge [μm]
G
Dendritic field area across lesion
4 months
2 months
1 month
2 weeks
1 week
Dendritic field area [μm²]
Distance to lesion edge [μm]

Figure 21. S-cone bipolar cells branch profusely in response to deafferentation. A. In a 2-month-old ablation zone, visible as a lack of iGluR5 (green) S-cone dendritic stalks show numerous dendritic branches (HCN4, cyan). Scale bar 100µm. B. Dendritic tree traces of A (black lines) shown with cell soma locations (black circles). S-cones (blue circles) exist outside the ablation zone (red line). Orange convex polygons outline the dendritic tree of two example cells. Polygon areas are used in G. C. The number of dendritic branches per cell with respect to the lesion edge. n refers to lesions included in analysis. In all cases, an n of 1 gives at least 30 cells inside (edge distance < 0) and outside the ablation zone. S-cone bipolar cells inside the ablation zone have more dendritic branches within the OPL than S-cone bipolar cells outside the ablation zone (binomial probability, 1 week p = 2e-4, 2 weeks p = 0.027, 1 month p = 0.035, 2 months p <1e-7, 4 months p = 5e-12). D. Schematic of deafferented S-cone bipolar cell. New dendrites form in the OPL (arrow). E. Example of deafferented S-cone bipolar cell. The single vertical dendritic stalk branches into two within the OPL (arrow). F. Most new dendritic branching begins within the OPL, branching outside the OPL is relatively unchanged. G. Dendritic field area with respect to lesion edge. Dendritic field areas calculated from convex polygons surrounding dendritic tree (see orange shapes in B for examples). Dendritic fields of deafferented cells are significantly larger in 1+ month old lesions (KS test, 1week p = 0.22, 2 weeks p = 0.68, 1 month p = 0.02, 2 months p <1e-3, 4 months p = 7e-13)

To confirm if dendritic branches emanated in any direction or instead exhibited a direction preference towards available photoreceptors outside the ablation zone we measured the vector sum of each cell's dendritic projections. We find that there is no orientation in the dendritic projection direction of cells inside the ablation zone (Figure 22).

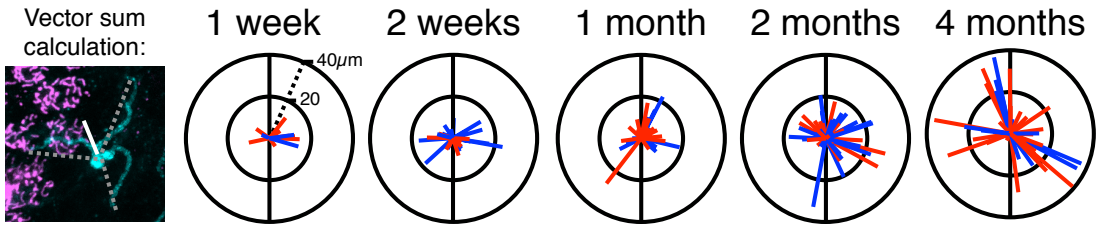

Figure 22. Dendritic projection vector sums of deafferented S-cone bipolar cells. Dendritic branch length and angle (dashed gray lines) of individual S-cone bipolar cells (cyan) were summed together (white line) for each cell. Angles were measured

with respect to lesion edge (visible as a lack of ribbons, magenta). Each line in the polar plots represents a single cell's dendritic vector sum. Cells to the right of the ablation zone center are colored red and cells to the left are blue. Lesions are oriented vertically in all plots (vertical black line).

S-cone bipolar cells sometimes find new S-cones

We next determined if deafferented S-cone bipolar cells find new S-cones. Most deafferented S-cone bipolar cells do not have dendrites that reach out of the ablation zone into the photoreceptor-rich areas (fraction). However, of the S-cone bipolar cells that do send dendrites outside the ablation zone, 40% of them make contact with S-cones (n = 30/77 edge cells in 1+ month old lesions, Figure 23A). If we look at the S-cones contacted by edge cells, we find that they are significantly more likely to diverge to more than one S-cone bipolar cell (Figure 23B, binomial test, 1 month $p=0.025$, 2 months $p=1e-6$, 4 months $p=0.002$).

S-cone bipolar cell dendrites that find new S-cones traveled within M-cone territory before finding their new partners. We find that dendrites will reach, on average 9µm into M-cone territory towards an S-cone, with some dendrites traveling much greater distances before contacting an S-cone (Figure 23C). We do not see a dependence on dendritic reach of successful edge cells with lesion age (KS test comparing 1 month dendritic reach to 2 and 4 month, all $p>0.19$).

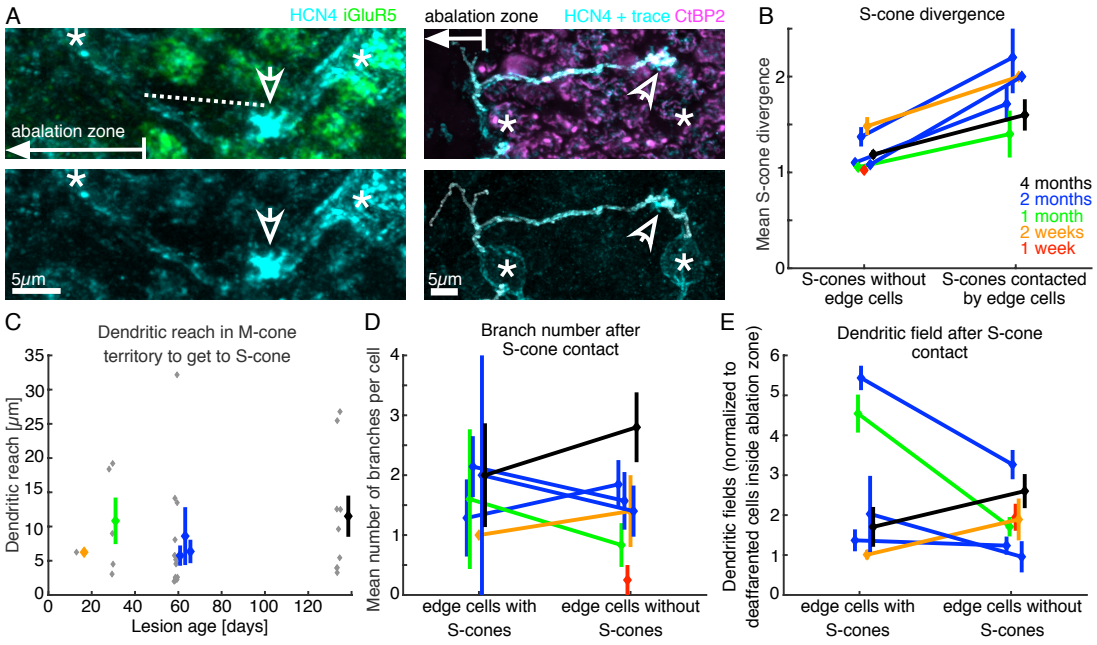

Figure 23. Deafferented S-cone bipolar cells near the ablation zone edge that successfully contact new S-cones.
A. Two examples of successful edge cells making contact with S-cones (arrows). In all panels, S-cone bipolar cell somas are marked with a (*). In both examples, one of the bipolar cell's dendritic field starts in the ablation zone (defined by a lack of iGluR5 (green) or ribbons (magenta)) and travel through M-cone territory to make contact with the S-cone. The dendritic reach through M-cone territory is defined by the dashed line. B. The divergence of S-cones that are contacted by edge cells and those that are not. C. The dendritic reach through M-cone territory of individual cells to make contact with an S-cone (gray dots). See dashed line in A for example of dendritic reach through M-cone territory. Mean +_ SEM of lesions shown in colors, slight offset from dots. D. The number of branches in edge cells with or without S-cones. Mean +- SEM. E. The dendritic field of edge cells with and without S-cones. The dendritic fields have been normalized to the dendritic fields of cells within the ablation of their respective lesions.

We next ask if S-cone bipolar cells ever missed an opportunity to connect with an S-cone. First, we determined if any non-presynaptic S-cones ever exist within the dendritic field of an S-cone bipolar cell. We described the dendritic field as a convex polygon around the dendrites that travel within the OPL of an S-cone bipolar

cell. We find that S-cones typically sit at a vertex of this convex polygon. We rarely observed S-cone bipolar cells that missed an S-cone within their dendritic field (n = 1/65 cells with dendritic fields overlapping the lesion edge). It is interesting to note that the single cell that missed one S-cone was not entirely unsuccessful; the same S-cone bipolar cell made contact with another S-cone within its dendritic field.

Deafferented S-cone bipolar cells that find S-cones do not simplify their dendritic trees

The mechanisms and strategies used by S-cone bipolar cells to find S-cones in the developing retina are unknown, however, we wanted to understand if the mechanisms used to find new synaptic partners in the adult retina are comparable to developmental mechanisms. We looked at the dendritic trees of deafferented S-cone bipolar cells that successfully found new S-cone pre-synaptic partners in the adult retina compared to their counterparts that found their pre-synaptic partners during development. S-cone bipolar cells in the healthy retina typically have a single dendritic stalk. However, we find that deafferented S-cone bipolar cells that have found an S-cone do not prune their additional dendritic branches (Figure 23D, binomial probability comparing deafferented edge cells with edge cells that find S-cones, 1 month $p=0.23$, 2 months $p=0.07$, 4 months $p=0.13$). Furthermore, the dendritic fields of rewired S-cone bipolar cells and deafferented S-cone bipolar cells at the lesion edge are indistinguishable from one another (Figure 23E, KS test, $p>0.36$). S-cone bipolar cells that find new S-cones in the adult retina do not simplify their dendritic tree back to a single stalk.

Deafferented Secretagogin- and CD15-positive bipolar cells simplify their dendritic trees

We used antibodies to secretagogin and CD15 to identify additional cone bipolar cell types in the ground squirrel retina after photoreceptor ablation. Secretagogin-positive bipolar cells (at least one ON and OFF type) lose their dendritic tips within 1 week of photoreceptor loss. The dendritic tips are normally located post-synaptically to cone pedicles (Figure 24A, B). CD15 positive bipolar cells (a single ON type) typically exhibit dendritic swellings post-synaptic to cones. The dendritic swellings disappear within 1 week and at 2 months the dendritic network appears disturbed (Figure 24C). Preliminary results looking at CD15-positive bipolar cells, whose dendritic trees can sometimes be traced in their entirety, do not exhibit increased branching as observed in the S-cone bipolar cells. Rather, deafferented CD15 cells may instead exhibit dendritic pruning.

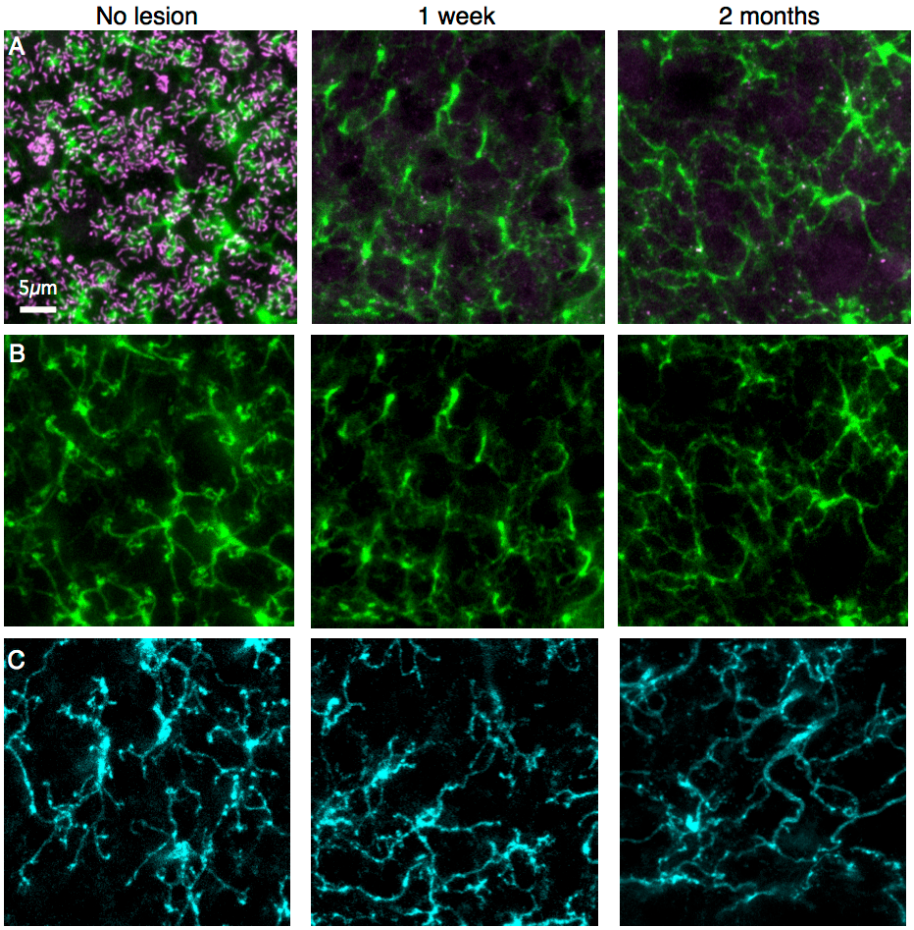

Figure 24. Dendritic tree changes in deafferented secretagogin- and CD15-stained bipolar cells.
A and B. Secretagogin-stained bipolar cells (green) outside the lesion have dendritic tips in contact with cone pedicles (CtBP2, magenta). 1-week post photoreceptor loss, ribbons are gone and dendritic tips have disappeared. 2-months post photoreceptor loss the dendritic network is disturbed. C. CD15-stained bipolar cells (cyan) lose their organized appearance with lesion age. Panels in C are from the same areas of retina in A and B, except for the 2-month-old panel, which comes from a different 2-month-old lesion.

Discussion

Deafferented S-cone bipolar cells in the adult ground squirrel retina expand their dendritic tree beyond a single stalk in search of new synaptic partners. The

dendritic tree expansion occurs within the correct layer of the retina, the outer plexiform layer. The new branches, formed in adulthood, start within the outer plexiform layer instead of closer to the cell soma, as we observe in healthy S-cone bipolar cells. In some cases, deafferented S-cone bipolar cells find new S-cone partners and travel through M-cone territory to do so. Successful deafferented S-cone bipolar cells do not prune their dendritic tree back to a single stalk to resemble healthy S-cone bipolar cells but instead maintain an expanded dendritic tree within the outer plexiform layer.

Precise synaptic connectivity in the adult retina

The S-cone bipolar cell, with its precise synaptic connectivity, is necessary for blue/yellow color vision in the ground squirrel retina. Here, we asked if deafferented S-cone bipolar cells, in the adult retina, are capable of recreating the precise circuitry required for color discrimination. Our findings show that precise circuitry formation in the adult retina, though possible, is limited. Although deafferented S-cone bipolar cells will significantly expand their dendritic tree in search of new pre-synaptic partners, many of the cells at the center of the ablation zone never extend their dendrites out of that zone, leaving them deafferented. The deafferented cells near the ablation zone edge send their dendrites into photoreceptor-rich areas; however, only 40% of them make contact with S-cones. We could not conclusively discern the connectivity or lack thereof of M-cones to S-cone bipolar cells. Evidence for mechanisms that allow for specific wiring in the adult animal come from the lengths that some deafferented S-cones go to find new S-cones, bypassing M-cones along the

way. On average, S-cone bipolar cells bypass two M-cone pedicles to find an S-cone (9µm average travel roughly translates to two 5µm diameter cone pedicles). S-cone bipolar cells do not simply contact the closest cone. This suggests selective wiring mechanisms exist in the adult retina but these mechanisms do not produce the same success rate as those that exist in the developing retina.

Plasticity mechanisms differ between cone bipolar cell types

Cone bipolar cells respond to local photoreceptor loss separately from one another. This is especially apparent in the differences we observe between S-cone bipolar cells and CD15 cells. S-cone bipolar cells branch prolifically, while CD15-positive cells do not. Furthermore, the plasticity strategies we observe between these two cell types in the ground squirrel also differ from our observations of rod bipolar cells in rabbit retina. It is possible, or even likely, the different strategies we observe are simply a product of species differences. However, recent experiments in the mouse retina indicate that mouse rod bipolar cells respond to photoreceptor loss in the same way as rabbit rod bipolar cells, hinting that structural plasticity mechanisms may be similar across species.

CONCLUSIONS and FUTURE DIRECTIONS

Discussion summary

In this thesis I have presented evidence for functional synaptogenesis in the adult retina. I explored how that synaptogenesis occurred and detailed the structural plasticity in the adult retina. I found that rewiring strategies differ across bipolar cell types and that correct synaptogenesis is possible but wiring selectivity is reduced in the adult retina. This research is especially relevant to photoreceptor reintroduction therapies and highlights the role bipolar cells will play in successful vision restoration.

Photoreceptor reintroduction studies have been focused on the photoreceptors and understandably so; introducing new photoreceptors into a degenerating retina presents a multitude of challenges (many of which are reviewed in (Pearson, 2014)). Despite the challenges, photoreceptor replacement seems achievable because photoreceptors "need only to make short, single synaptic connections to the remaining inner retinal circuitry to contribute to visual function" (Pearson, 2014). This photoreceptor-focused philosophy, albeit unintentionally, exhibits bipolar cells in a passive role waiting for photoreceptor rescue. I show that bipolar cells, not photoreceptors, initiate synaptogenesis.

The plasticity mechanisms available to adult bipolar cells are promising for vision rescue strategies but they do not perfectly mimic the developing retina's precision in forming new circuitry. Imprecise circuitry will result in the loss of parallel pathways, which are necessary for proper vision. Future therapies will need to

address this lack of precision to achieve perfect vision rescue. The distinct plasticity mechanisms between bipolar cell types will probably complicate future therapeutic strategies; parallel pathways may have to be addressed individually.

Future directions

Cellular mechanisms behind plasticity

The mechanisms behind the synaptogenesis and plasticity in the adult retina remain unknown. It is unlikely that the imprecise wiring issue will be successfully addressed in future therapies without knowing the mechanisms behind the innate rewiring. The genetic control and relative wealth of knowledge make the mouse the best animal model for mechanism discovery. To this end, photocoagulation experiments in mice have already begun in the Sher lab. Preliminary findings suggest that rod bipolar cells in mouse exhibit a phenotype similar to rod bipolar cells in the rabbit retina; rod bipolar cell dendrites direct themselves out of the ablation zone. A mouse missing ELFN1, which shows normal rod bipolar cell dendritic trees but lacks synapses between rods and rod bipolar cells in the adult retina will be investigated for its ability to seek out new photoreceptors after selective local ablation (Cao et al., 2015).

Adult plasticity mechanisms and developmental wiring strategies

It is unknown if the adult retina uses developmental mechanisms and strategies to rewire or if the adult retina has access to a different set of mechanisms. It

is possible to explore this question without waiting for the exact mechanisms to be pinpointed. Instead, deafferented bipolar cells can be compared to their developing counterparts. In the healthy developing mouse retina, three cone bipolar cell types use distinct strategies from one another to find and refine their circuitry (Dunn and Wong, 2012). The three cone bipolar cell types are readily comparable because of the existence of established mouse lines that specifically and sparsely label the three individual bipolar cell types. It would be relatively straightforward to use these mice for photocoagulation experiments and compare the adult bipolar cell rewiring strategies to their developmental wiring strategies.

Bipolar cell plasticity after photoreceptor reintroduction

The motivation behind investigating adult retinal plasticity stems from the promise of future photoreceptor reintroduction therapies to restore vision. Photoreceptor reintroduction experiments are the next step in this investigation. Dr. Daniel Palanker's lab is developing a technique to place a sheet of photoreceptors into an adult retina. The techniques and procedures used throughout this thesis are readily applicable to this next phase of the project. The Sher lab will investigate the functional and structural changes that occur within the host retina and shed light on the future of vision restoration.

REFERENCES

Baden T, Berens P, Franke K, Roman-Roson M, Bethge M, Euler (2016) The functional diversity of mouse retinal ganglion cells. Nature 529:345–350.

Barhoum R, Martínez-Navarrete G, Corrochano S, Germain F, Fernandez-Sanchez L, de la Rosa EJ, de la Villa P, Cuenca N (2008) Functional and structural modifications during retinal degeneration in the rd10 mouse. Neuroscience 155:698–713.

Beier C, Hovhannisyan A, Weiser S, Kung J, Lee S, Yeong Lee D, Huie P, Dalal R, Palanker D, Sher A (2017) Deafferented adult rod bipolar cells create new synapses with photoreceptors to restore vision. J Neurosci 37:2570–16.

Burns ME, Baylor DA (2001) activation , Deactivation , and adaptation in Vertebrate Photoreceptor Cells. Annu Rev Neurosci 24:779–805.

Busch EM, Gorgels TG, Van Norren D (1999) Filling-in after focal loss of photoreceptors in rat retina. Exp Eye Res 68:485–492.

Cao Y, Sarria I, Fehlhaber KE, Kamasawa N, Orlandi C, James KN, Hazen JL, Gardner MR, Farzan M, Lee A, Baker S, Baldwin K, Sampath AP, Martemyanov KA (2015) Mechanism for Selective Synaptic Wiring of Rod Photoreceptors into the Retinal Circuitry and Its Role in Vision. Neuron 87:1248–1260.

Chichilnisky EJ (2001) A simple white noise analysis of neuronal light. 12:199–213.

Claes E, Seeliger M, Michalakis S, Biel M, Humphries P, Haverkamp S (2004) Morphological Characterization of the Retina of the CNGA3-/-Rho-/- Mutant Mouse Lacking Functional Cones and Rods. Invest Ophthalmol Vis Sci 45:2039–2048.

Cuenca N, Pinilla I, Sauvé Y, Lu B, Wang S, Lund RD (2004) Regressive and reactive changes in the connectivity patterns of rod and cone pathways of P23H transgenic rat retina. Neuroscience 127:301–317.

Cuenca N, Pinilla I, Sauvé Y, Lund R (2005) Early changes in synaptic connectivity following progressive photoreceptor degeneration in RCS rats. Eur J Neurosci 22:1057–1072.

D'Orazi FD, Suzuki SC, Wong RO (2014) Neuronal remodeling in retinal circuit assembly, disassembly, and reassembly. Trends Neurosci 37:594–603.

Dacheux RF, Raviola E (1986) The rod pathway in the rabbit retina: a depolarizing bipolar and amacrine cell. J Neurosci 6:331–345.

Demb JB, Singer JH (2012) Intrinsic properties and functional circuitry of the AII amacrine cell. Biophys Chem 257:2432–2437.

Dhande OS, Stafford BK, Lim J-HA, Huberman AD (2015) Contributions of Retinal Ganglion Cells to Subcortical Visual Processing and Behaviors. Annu Rev Vis Sci 1:291–328.

Dunn F a. (2015) Photoreceptor Ablation Initiates the Immediate Loss of Glutamate Receptors in Postsynaptic Bipolar Cells in Retina. J Neurosci 35:2423–2431.

Dunn FA, Wong ROL (2012) Diverse Strategies Engaged in Establishing Stereotypic Wiring Patterns among Neurons Sharing a Common Input at the Visual System ' s First Synapse. J Neurosci 32:10306–10317.

Euler T, Haverkamp S, Schubert T, Baden T (2014) Retinal bipolar cells: elementary building blocks of vision. Nat Rev Neurosci 15:507–519.

Field GD, Sher A, Gauthier JL, Greschner M, Shlens J, Litke AM, Chichilnisky EJ (2007) Spatial properties and functional organization of small bistratified ganglion cells in primate retina. J Neurosci 27:13261–13272.

Haverkamp S, Michalakis S, Claes E, Seeliger MW, Humphries P, Biel M, Feigenspan A (2006) Synaptic plasticity in CNGA3(-/-) mice: cone bipolar cells react on the missing cone input and form ectopic synapses with rods. J Neurosci 26:5248–5255.

Jones BW, Kondo M, Terasaki H, Lin Y, McCall M, Marc RE (2012) Retinal remodeling. Jpn J Ophthalmol 56:289–306.

Jones BW, Marc RE (2005) Retinal remodeling during retinal degeneration. Exp Eye Res 81:123–137.

Jones BW, Watt CB, Frederick JM, Baehr W, Chen C-K, Levine EM, Milam AH, Lavail MM, Marc RE (2003) Retinal remodeling triggered by photoreceptor degenerations. J Comp Neurol 464:1–16.

Kolb H, Fernandez E, Nelson R (2016) Webvision: The Organization of the Retina and Visual System. :http://www.ncbi.nlm.nih.gov/books/NBK11504/.

Lavinsky D, Cardillo J a, Mandel Y, Huie P, Melo L a, Farah ME, Belfort R, Palanker D (2013) Restoration of retinal morphology and residual scarring after

photocoagulation. Acta Ophthalmol:1–9.

Legland D, Arganda-Carreras I, Andrey P (2016) MorphoLibJ: integrated library and plugins for mathematical morphology with ImageJ. Bioinformatics 32:btw413.

Li W, DeVries SH (2004) Separate blue and green cone networks in the mammalian retina. Nat Neurosci 7:751–756.

Li W, DeVries SH (2006) Bipolar cell pathways for color and luminance vision in a dichromatic mammalian retina. Nat Neurosci 9:669–675.

Li W, Keung JW, Massey SC (2004) Direct synaptic connections between rods and OFF cone bipolar cells in the rabbit retina. J Comp Neurol 474:1–12.

Litke A, Bezayiff N, Chichilnisky EJ, Sher A (2004) What does the eye tell the brain?: Development of a system for the large-scale recording of retinal output activity. Nucl Sci 51:1434–1440.

Longair MH, Baker DA, Armstrong JD (2011) Simple neurite tracer: Open source software for reconstruction, visualization and analysis of neuronal processes. Bioinformatics 27:2453–2454.

Lorach H, Kung J, Beier C, Mandel Y, Dalal R, Huie P, Wang J, Lee S, Sher A, Jones BW, Palanker D (2015) Development of Animal Models of Local Retinal Degeneration. Investig Opthalmology Vis Sci 56:4644.

MacLaren RE, Pearson R a, MacNeil a, Douglas RH, Salt TE, Akimoto M, Swaroop a, Sowden JC, Ali RR (2006) Retinal repair by transplantation of photoreceptor precursors. Nature 444:203–207.

Marc RE, Jones BW (2002) Molecular phenotyping of retinal ganglion cells. J Neurosci 22:413–427.

Marc RE, Jones BW, Watt CB, Strettoi E (2003) Neural remodeling in retinal degeneration. Prog Retin Eye Res 22:607–655.

Masland RH (2012) The Neuronal Organization of the Retina. Neuron 76:266–280.

Michalakis S, Schäferhoff K, Spiwoks-Becker I, Zabouri N, Koch S, Koch F, Bonin M, Biel M, Haverkamp S (2012) Characterization of neurite outgrowth and ectopic synaptogenesis in response to photoreceptor dysfunction. Cell Mol Life Sci.

NEI (n.d.) Age-Related Macular Degeneration (AMD) | National Eye Institute.

Available at: https://nei.nih.gov/health/maculardegen [Accessed May 8, 2017a].

NEI (n.d.) Facts About Retinitis Pigmentosa | National Eye Institute. Available at: https://nei.nih.gov/health/pigmentosa/pigmentosa_facts [Accessed May 8, 2017b].

Pan F, Massey SC (2007) Rod and Cone Input to Horizontal Cells. 831:815–831.

Paulus YM, Jain A, Gariano RF, Stanzel B V, Marmor M, Blumenkranz MS, Palanker D (2008) Healing of retinal photocoagulation lesions. Invest Ophthalmol Vis Sci 49:5540–5545.

Paulus YM, Jain A, Nomoto H, Sramek C, Gariano RF, Andersen D, Schuele G, Leung L-S, Leng T, Palanker D (2011) Selective retinal therapy with microsecond exposures using a continuous line scanning laser. Retina 31:380–388.

Pearson R a. (2014) Advances in repairing the degenerate retina by rod photoreceptor transplantation. Biotechnol Adv 32:485–491.

Peng YW, Hao Y, Petters RM, Wong F (2000) Ectopic synaptogenesis in the mammalian retina caused by rod photoreceptor-specific mutations. Nat Neurosci 3:1121–1127.

Preibisch S, Saalfeld S, Tomancak P (2009) Globally optimal stitching of tiled 3D microscopic image acquisitions. Bioinformatics 25:1463–1465.

Puller C, Ondreka K, Haverkamp S (2011) Bipolar cells of the ground squirrel retina. J Comp Neurol 519:759–774.

Puthussery T, Gayet-Primo J, Taylor WR (2010) Localization of the calcium-binding protein secretagogin in cone bipolar cells of the mammalian retina. J Comp Neurol 518:513–525.

Rowe MH (2002) Trichromatic color vision in primates. News Physiol Sci 17:93–98.

Sanes JR, Masland RH (2014) The Types of Retinal Ganglion Cells: Current Status and Implications for Neuronal Classification. Annu Rev Neurosci 38:150421150146009.

Schindelin J, Arganda-Carreras I, Frise E, Kaynig V, Longair M, Pietzsch T, Preibisch S, Rueden C, Saalfeld S, Schmid B, Tinevez J-Y, White DJ, Hartenstein V, Eliceiri K, Tomancak P, Cardona A (2012) Fiji: an open-source platform for biological-image analysis. Nat Methods 9:676–682.

Sher A, Devries SH (2012) A non-canonical pathway for mammalian blue-green color vision. Nat Neurosci 15:952–953.

Sher A, Jones BW, Huie P, Paulus YM, Lavinsky D, Leung L-SS, Nomoto H, Beier C, Marc RE, Palanker D (2013) Restoration of Retinal Structure and Function after Selective Photocoagulation. J Neurosci 33:6800–6808.

Singh MS, MacLaren RE (2011) Stem cells as a therapeutic tool for the blind: biology and future prospects. Proc Biol Sci 278:3009–3016.

Stasheff SF, Shankar M, Andrews MP (2011) Developmental time course distinguishes changes in spontaneous and light-evoked retinal ganglion cell activity in rd1 and rd10 mice. J Neurophysiol 105:3002–3009.

Strazzeri JM, Hunter JJ, Masella BD, Yin L, Fischer WS, Diloreto D a, Libby RT, Williams DR, Merigan WH (2014) Focal damage to macaque photoreceptors produces persistent visual loss. Exp Eye Res 119:88–96.

Strettoi E, Mears AJ, Swaroop A (2004) Recruitment of the rod pathway by cones in the absence of rods. J Neurosci 24:7576–7582.

Strettoi E, Pignatelli V (2000) Modifications of retinal neurons in a mouse model of retinitis pigmentosa. Proc Natl Acad Sci U S A 97:11020–11025.

Strettoi E, Pignatelli V, Rossi C, Porciatti V, Falsini B (2003) Remodeling of second-order neurons in the retina of rd/rd mutant mice. Vision Res 43:867–877.

Sullivan RKP, WoldeMussie E, Pow D V. (2007) Dendritic and Synaptic Plasticity of Neurons in the Human Age-Related Macular Degeneration Retina. Investig Opthalmology Vis Sci 48:2782.

tom Dieck S, Altrock WD, Kessels MM, Qualmann B, Regus H, Brauner D, Fejtová A, Bracko O, Gundelfinger ED, Brandstätter JH (2005) Molecular dissection of the photoreceptor ribbon synapse: Physical interaction of Bassoon and RIBEYE is essential for the assembly of the ribbon complex. J Cell Biol 168:825–836.

Vaney DI, Sivyer B, Taylor WR (2012) Direction selectivity in the retina: symmetry and asymmetry in structure and function. Nat Rev Neurosci 13.

Vardi N, Duvoisin R, Wu G, Sterling P (2000) Localization of mGluR6 to dendrites of ON bipolar cells in primate retina. J Comp Neurol 423:402–412.

Wässle H (2004) Parallel processing in the mammalian retina. Nat Rev Neurosci 5:747–757.

Wässle H, Puller C, Müller F, Haverkamp S (2009) Cone contacts, mosaics, and territories of bipolar cells in the mouse retina. J Neurosci 29:106–117.

Young HM, Vaney DI (1991) Rod-signal interneurons in the rabbit retina: 1. Rod bipolar cells. J Comp Neurol 310:139–153.